International Journal of Extreme Manufacturing

Functional microfluidics: theory, microfabrication, and applications

OPEN ACCESS
IOP Publishing | IMMT
International Journal of Extreme Manufacturing
Int. J. Extrem. Manuf. **6** (2024) 032005 (34pp)
https://doi.org/10.1088/2631-7990/ad2c5f

Topical Review

Functional microfluidics: theory, microfabrication, and applications

Mingzhu Xie[1], Ziheng Zhan[1], Yinfeng Li[1], Junkai Zhao[2,3], Ce Zhang[3,*], Zhaolong Wang[1,*] and Zuankai Wang[4,*]

[1] Interdisciplinary Research Center of Low-carbon Technology and Equipment, College of Mechanical and Vehicle Engineering, Hunan University, Changsha 410082, People's Republic of China
[2] Energy Research Institute of Shandong Academy of Sciences, Qilu University of Technology (Shandong Academy of Sciences), Jinan 250014, People's Republic of China
[3] Qian Xuesen Laboratory of Space Technology, China Academy of Space Technology (CAST), Beijing 100094, People's Republic of China
[4] Department of Mechanical Engineering, Hong Kong Polytechnic University, Hong Kong Special Administrative Region of China 999077, People's Republic of China

E-mail: zhangce-qxslab@outlook.com, zhaolongwang@hnu.edu.cn and zk.wang@polyu.edu.hk

Received 29 June 2023, revised 5 September 2023
Accepted for publication 22 February 2024
Published 19 March 2024

Abstract

Microfluidic devices are composed of microchannels with a diameter ranging from ten to a few hundred micrometers. Thus, quite a small (10^{-9}–10^{-18} l) amount of liquid can be manipulated by such a precise system. In the past three decades, significant progress in materials science, microfabrication, and various applications has boosted the development of promising functional microfluidic devices. In this review, the recent progress on novel microfluidic devices with various functions and applications is presented. First, the theory and numerical methods for studying the performance of microfluidic devices are briefly introduced. Then, materials and fabrication methods of functional microfluidic devices are summarized. Next, the recent significant advances in applications of microfluidic devices are highlighted, including heat sinks, clean water production, chemical reactions, sensors, biomedicine, capillaric circuits, wearable electronic devices, and microrobotics. Finally, perspectives on the challenges and future developments of functional microfluidic devices are presented. This review aims to inspire researchers from various fields—engineering, materials, chemistry, mathematics, physics, and more—to collaborate and drive forward the development and applications of functional microfluidic devices, specifically for achieving carbon neutrality.

Keywords: capillary theory, functional devices, functional microfluidics, future in carbon neutrality, microfabrication methods

* Authors to whom any correspondence should be addressed.

2631-7990/24/032005+34$33.00

1. Introduction

Microfluidic phenomena with micro/nanoscale features based on the capillary force were first discovered by da Vinci [1]. In 1718, Jurin [2] proposed the famous Jurin criterion, demonstrating the inversely proportional relationship between the height of the liquid and the diameter of the microtubes. In 1751, Segner [3] discovered the surface tension of fluids. In 1806, Thomas Young and Pierre Simon Laplace [4] independently deduced the relationship between the additional pressure of the curved liquid surface, surface tension, and the radius of curvature of the liquid based on the wettability theory for the liquid/solid interface. Subsequently, Gauss [5] modified the capillary theory based on an energy analysis in 1830. Gibbs [6] considered free energy and chemical potential within the framework of thermodynamics (figure 1). However, those famous theories on capillary phenomena can only be applied to the ideal circular microchannels, and numerous simulation methods were thus applied to the theoretical analysis of microfluidics with the fast development of computers, such as the computational fluid dynamics (CFD) method [7], the molecular dynamics (MD) method [8], as well as several mesoscopic methods such as the lattice Boltzmann method (LBM) [9] and the direct simulation Monte Carlo method [10].

Meanwhile, the great demand for microfluidic devices is severely limited by the fabrication methods. Blowing glass tubes and parallel plates were commonly used to validate these proposed theories before Terry *et al* [11] performing a gas chromatographic air analyzer on a silicon substrate in 1979, ushering in the era of fabrication for microchannels based on lithography of silicon. In 1990, Manz *et al* [12] achieved the miniaturized total chemical analysis systems based on a silicon-based microfluidic chip, which is regarded as the prototype of functional microfluidic devices. However, the shortcomings of expensive and limited applications of silicon-based microchannels arouse the fast development of materials and fabrication methods for microfluidic devices afterward. Microfluidic systems based on polydimethylsiloxane (PDMS) were first developed by Mcdonald *et al* [13] in 2000. Then, various new materials were introduced to the fabrication of microchannels, such as polymethylmethacrylate (PMMA) [14], epoxy resins [15], hydrogels [16–18], and other plastics [19]. However, these materials and traditional fabrication methods are limited to two-dimensional (2D) microchannels, including the popular patterned paper [20]. In 2018, Yuan *et al* [21] fabricated structured multimaterial fibers with complex cross-shapes by using a thermal drawing process. With the fast development of three-dimensional (3D) printing techniques [22–24], more and more microfluidic devices are fabricated with such an advanced technique. In 2023, Wang *et al* [25] fabricated a bionic microfluidic device with arbitrarily shaped and sized microchannels based on projection microstereolithography (SLA) based 3D printing technique.

The fast development of the theory and fabrication methods for microchannels drastically drives their applications. In 2006, Whitesides [26] predicted the future development of microfluidics, pointing out that microfluidics devices can be used in many fields, including screen conditions, manipulation of multiphase flows, chemical synthesis, cell biology, and microanalytical devices. He also pointed out that the future development of microfluidics would be in the design and manufacturing systems for microfluidic devices. Due to the merits of microchannels, such as compactness, microscale, and ease of integration discovered in the past few decades [26], the applications of microfluidic devices have been also boosted in various fields, such as heat sinks [27], heat transport [28], diagnostics [29], detection [30], biomedical engineering [31], production of materials [32], and reactors [33]. Recently, more and more complex microfluidic devices have been proposed [34], including capillaric circuits [35], wearable electronic devices [36], microrobotics [37, 38], and triboelectric generators [39, 40].

Over time, functional microfluidics referring to the integration of various components and functionalities to perform specific tasks and functions has achieved a lot in the past century. They are designed to not only manipulate fluid flow but also incorporate additional features such as sensing, mixing, separation, reaction, and detection capabilities. Functional microfluidics enables more complex and versatile operations, allowing for a wide range of applications in various fields like chemistry, biology, medicine, engineering, and so on. However, there are still many deficiencies in microfluidics which severely limit their further development, especially in materials, fabrication of scale-up microfluidic devices, programmability of functional microfluidic devices, and so on. Herein, in this review, we summarize the recent progress in functional microfluidics from theory, fabrication methods to various promising applications. First, we briefly introduce the theories and numerical methods for studying transport phenomena in microfluidics. Then, we focus on the manufacturing methods of functional microfluidic devices simultaneously considering categories and materials. Also, the recent significant advances in its applications for microfluidic devices in various fields are highlighted. Finally, we provide personal perspectives on the challenges and future trends of functional microfluidic devices, especially in their applications on carbon neutrality.

2. Theoretical developments of microfluidics

2.1. Interface and theory for the wettability

Wetting of liquids on solid surfaces is a common phenomenon in nature [41–43]. The main factors affecting the wettability of a solid surface are its chemical composition and roughness [44–46]. With the development of technology over the past decades, the wettability of a solid surface has been studied extensively. As shown in figure 2, there are superhydrophilic, superhydrophobic, superoleophilic, and superoleophobic phenomena in air, superoleophobicity, superoleophilicity, superaerophobicity, superaerophilicity, and superhydrophilic phenomena underwater, as well as superhydrophobic phenomena in oil [47]. To classify the wettability of different kinds of surfaces, a series of theories from Young's equation to the Wenzel and Cassie–Baxter models have been established.

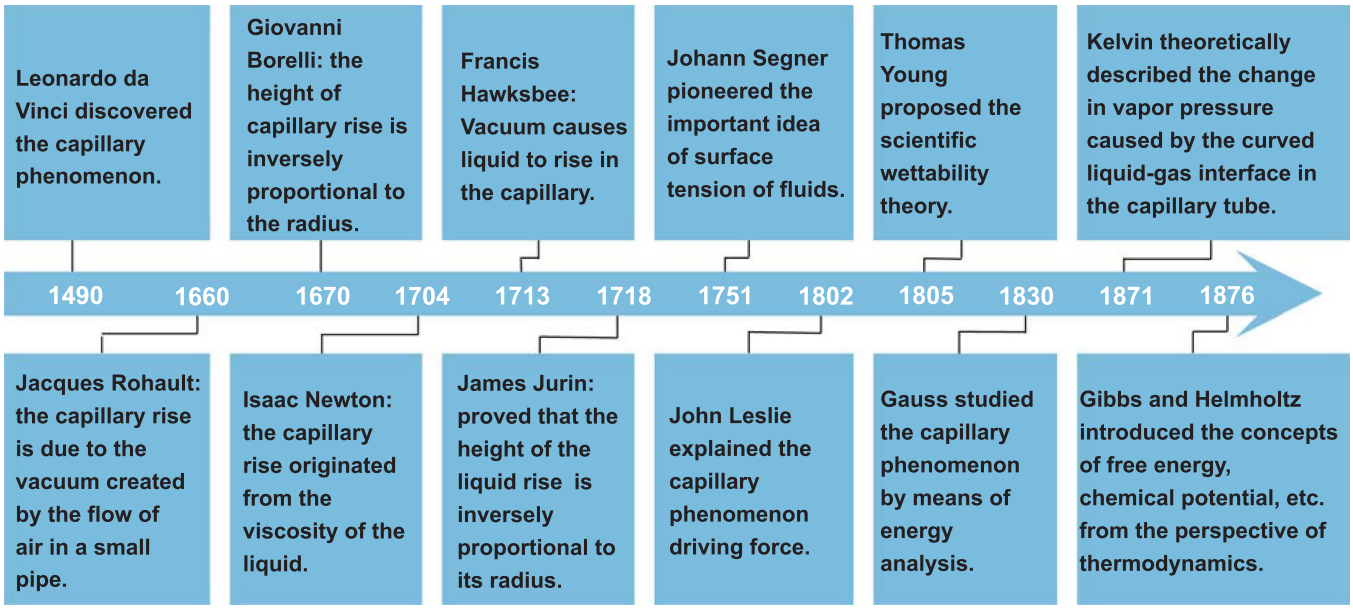

Figure 1. The history of capillary phenomena.

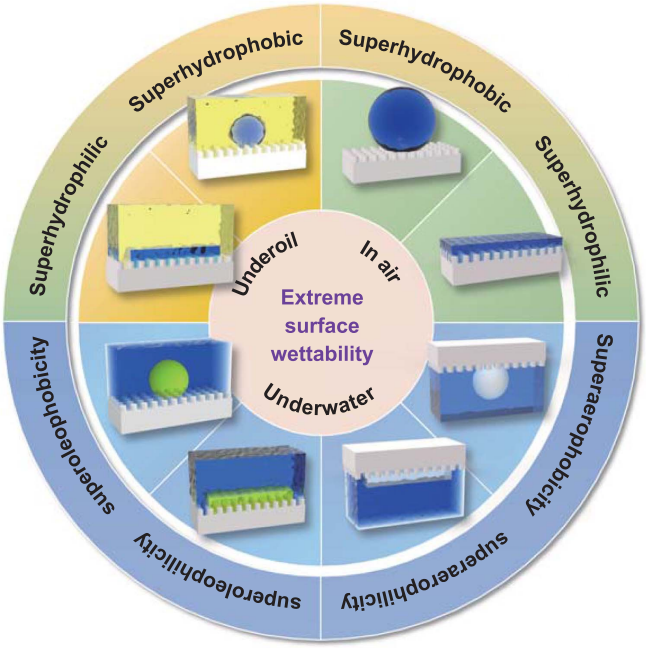

Figure 2. Wettability, including superhydrophilic, superhydrophobic, superoleophilic, and superoleophobic phenomena when the surfaces are in the air. Derived superoleophobicity, superoleophilicity, superaerophobicity, and superaerophilicity when the surfaces are underwater. Achieved wettability cases, such as superhydrophilic and superhydrophobic surfaces are in oil.

For smooth surfaces under equilibrium at the interface of solid and liquid (figure 3(a)), Young's equation describes the relationship between the solid–gas (γ_{SG}), solid–liquid (γ_{SL}), and liquid–gas (γ_{LG}) interfacial tensions to the static contact angle (θ) as follows [48]:

$$\gamma_{SG} = \gamma_{SL} + \gamma_{LG}\cos\theta. \tag{1}$$

The static contact angle is a quantitative characterization of the surface wettability [49]. It is expressed as the angle between the liquid/vapor interface to the solid surface when the liquid contacts with a solid surface. However, the static contact angle is not enough because the contact angle of an actual surface fluctuates under the action of external forces [50]. For a moving droplet, the maximum and minimum contact angles are called advancing (figure 3(b)) and receding (figure 3(c)) contact angles, respectively. Moreover, a smooth surface does not exist in reality, thus the effects of solid surface's roughness on its contact angle must be considered. For rough surfaces with uniformly distributed microstructures, the commonly used models for illustrating their contact angles are the Wenzel and Cassie–Baxter models. In the Wenzel model [51], the gaps between microstructures are assumed to be uniformly distributed, who are filled with liquid (figure 3(d)). Thus, the surface roughness (R_0) is introduced to characterize its effects on the static contact angle of rough surfaces. The modified contact angle can be expressed as

$$\cos\theta^* = R_0\cos\theta \tag{2}$$

where θ^* and θ are the contact angles of rough (after correction) and smooth surfaces, respectively. R_0 is the roughness of a surface (for rough surfaces, R_0 is invariably greater than 1). Generally speaking, the rougher the surface is, the greater the hydrophilicity or hydrophobicity. However, for some surfaces with extremely-high roughness, the absolute value of the right-hand side of the foregoing equation (2) exceeds 1. Under such circumstances, the Wenzel model fails, and the Cassie–Baxter model is developed with a series of corrections based on the Wenzel model.

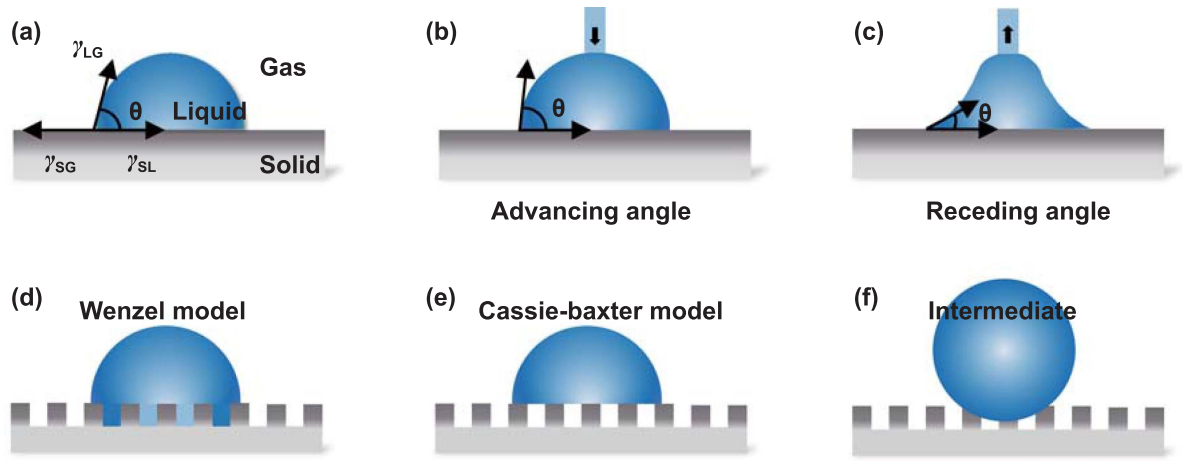

Figure 3. Wettability of solid surfaces. (a) The mechanical force balance on three-phase contact line in Young's equation. Schematic of (b) advancing contact angle and (c) receding contact angle. (d) Wenzel model. (e) Cassie–Baxter model. (f) Intermediate states of Wenzel and Cassie–Baxter models.

In the Cassie–Baxter model [52], the assumption is that the microstructures on a solid surface are not penetrated by the liquid. Instead, it is treated as a composite surface (figure 3(e)). Hence, the states are divided into two cases, solid–liquid contact and gas–liquid contact. The expression for such a phenomenon is

$$\cos\theta^* = f_s \cos\theta_s + f_g \cos\theta_g \tag{3}$$

where f_s and f_v represent the ratios of the areas in the solid–liquid contact and gas–liquid contact to the total contact area, respectively. In this case, assuming that the contact angle at the gas–liquid interface is 180°, the Cassie–Baxter model yields the following:

$$\cos\theta^* = f_s(\cos\theta_s + 1) - 1. \tag{4}$$

The superhydrophobicity of a rough solid surface is well explained by the Cassie–Baxter model. That is, the superhydrophobicity appears when the ratio of the solid–liquid contact area to the total contact area is extremely small. Moreover, an intermediate state in which the liquid is partially submerged on a rough surface is shown in figure 3(f) [53]. However, the foregoing model is derived under ideal conditions, and many problems are encountered in practical applications. In subsequent, the Wenzel and Cassie models are found capable of transforming and coexisting under certain conditions [54]. With the development of these surface wettability theories, the wettability of many biologically inspired surfaces with special microstructures has been fully investigated [55]. These unique characteristics include the fluid harvesting properties of caninervis (figure 4(a)) [56], cactus spines (figure 4(b)) [57], and desert beetles (figure 4(c)) [58], the superhydrophobic properties of *Salvinia molesta* leaf (figure 4(d)) [59], butterfly wings (figure 4(e)) [60], and water strider legs (figure 4(f)) [61], as well as the fluid self-transport properties of *Nepenthes alata* (figure 4(g))[62], spider silk (figure 4(h)) [63], and shorebirds (figure 4(i)) [64]. All the foregoing unique surfaces in nature are inextricably linked to surface wettability theories.

2.2. Driving force and hydrodynamics inside microchannels

The capillary circulation in the early renaissance and the modern capillary action in the micro/nano-field was first discovered by Leonardo da Vinci, which is commonly found in all aspects of life (figure 1). Typically, the capillary circulation phenomenon can be simplified as a fine microchannel being vertically inserted into liquid. Based on the theory of surface wettability, the liquid wets the wall of the microchannels and rises inside of them, while the liquid that cannot wet the wall of the microchannels drops inside. Such a fluid transport behavior enabled by the capillary force is called the capillary phenomenon [65]. In 1718, Jurin [2] proved that the height of the liquid in microchannels is inversely proportional to their diameters, which is the famous Jurin criterion:

$$h = \frac{2\gamma\cos\theta}{\rho g r} \tag{5}$$

where h is the height of capillary rise or fall, γ is the surface tension of liquid, r is the radius of the capillary tube, ρ is the liquid density, g is the gravitational acceleration.

In addition, the Gaussian capillary equation related to the perimeter and area can be applied to calculate the curvature of the end concave liquid surface to obtain the capillary rise height [66]. Furthermore, Kelvin [67] theoretically described the change in vapor pressure caused by the curved liquid–gas interface in microchannels,

$$R_g T \ln\frac{p_r}{P_0} = 2\frac{\gamma M}{\rho R_d} \tag{6}$$

where R_g, T represent the gas constant and the thermodynamic temperature, respectively. P_r, P_0 are the saturated vapor pressure of the droplet and the plane liquid, respectively. γ is the surface tension of the liquid, M is the molar mass and R_d is the radius of a droplet.

The equation (6) explains various microfluidic phenomena, such as capillary adsorption, coalescence, and meniscus radius. Previous studies on the capillary phenomena are mostly

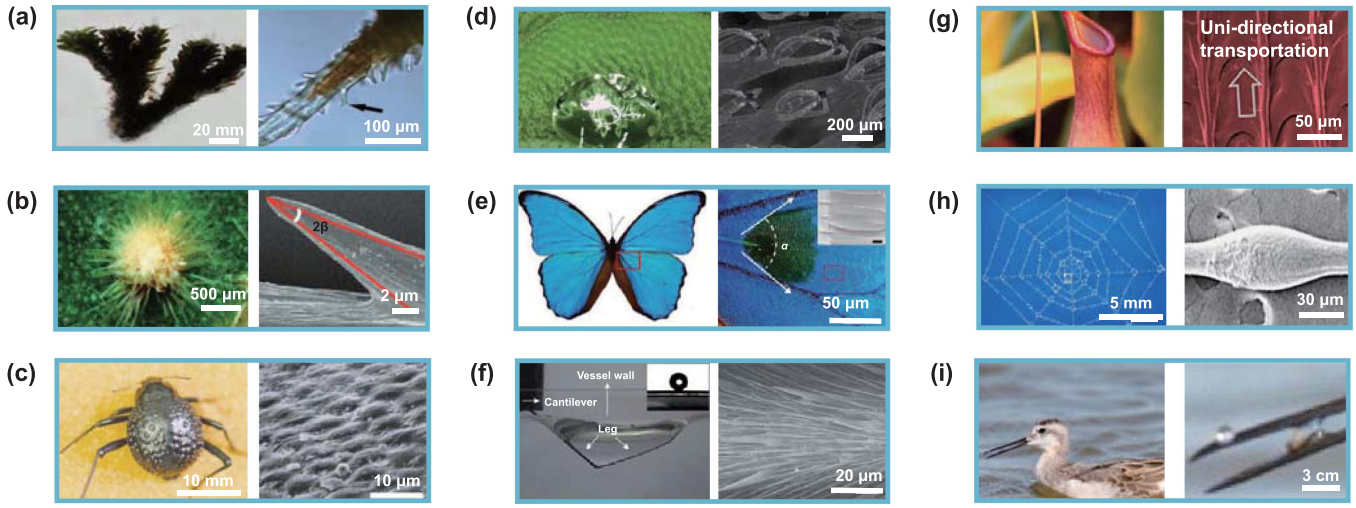

Figure 4. Bioinspired functional surfaces with specific microstructures based on surface wettability. Fluid harvesting properties of (a) caninervis [56]. [56] [Published online: 1 April 2011], reprinted by permission of the publisher (Taylor & Francis Ltd, www.tandfonline.com.). (b) Cactus spines [57]. Reproduced from [57], with permission from Springer Nature. (c) Desert beetles [58]. Reproduced from [58], with permission from Springer Nature. Superhydrophobic properties of (d) *S. molesta* leaves [59]. Reproduced from [59]. Used with permission of The Royal Society (U.K.), from [59]; permission conveyed through Copyright Clearance Center, Inc. (e) Butterfly wings [60]. [60] John Wiley & Sons. © 2023 Wiley-VCH GmbH. (f) Legs of water striders [61]. Reproduced from [61], with permission from Springer Nature. Fluid transport properties of (g) *N. alata* [62]. [62] John Wiley & Sons. [© 2018 WILEY-VCH Verlag GmbH & Co. KGaA, Weinheim]. (h) Spider silk [63]. Reproduced from [63]. CC BY 4.0. (i) Shorebirds [64]. From [64]. Reprinted with permission from AAAS.

discussed from the perspective of hydrostatics. In contrast, the steady-state flow of the liquid in microchannels can be approximated as Hagen–Poiseuille flow,

$$\frac{1}{r}\frac{d}{dr}\left(r\frac{dv}{dr}\right)=\frac{1}{\eta}\frac{\partial P}{\partial z} \tag{7}$$

where v is the flow velocity along the tube length (z-axis), and η is the viscosity of the fluid. In 1921, Washburn derived the relationship between the horizontal transport distance of liquid and the time in the initial stage of capillary rise based on Poiseuille's law for porous media [68],

$$h^2=\frac{cr\gamma\cos\theta t}{2\eta} \tag{8}$$

where c is the capillary shape factor, and t is the duration of the capillary rise process. The whole process will be greatly affected by capillary force, gravity, inertia force, and viscous force at different stages, where the capillary force is the driving force while the rest forces are the resistance terms.

Capillary force enables the long-distance transport of liquids (figure 5(a)) [69]. Recently, the involvement of external forces in microfluidics is attracting more and more attention [70, 71]. For example, electric field forces have been added to the microfluidic devices, including electrically induced wetting, liquid flow, and droplet motion enabled by charges [72, 73] (figure 5(b)). In addition, liquid motion can also be achieved by the momentum carried by photons transferred to the surface of the liquid, which is also known as radiation pressure (figure 5(c)) [74]. Moreover, light-induced capillary forces can be used to generate wettability gradients and Marangoni effects to drive the fluids. Also, a moving magnet can be used to control the movement of droplets containing magnetic particles (figure 5(d)) [75]. The advantages of magnetic driving force over electric driving force are that they can be operated manually without an additional external power supply. Furthermore, surface acoustic waves are also used in microfluidic devices for the manipulation of cells and particles owing to their simplicity, low cost, fast fluid drive, and broad compatibility (figure 5(e)) [76].

2.3. *Simulation methods for functional microfluidic phenomena*

In general, capillary theories with analytical solutions can only be applied to a few special situations. In addition, the experimental study of capillary phenomena strongly depends on the highly precise processing and fabrication of micro/nanochannels, leading to a fact that the results obtained from theory and experiments are inconsistent with each other, though the trends are similar to each other [77]. Therefore, numerous simulation methods (table 1) have been proposed to reveal the underlying mechanisms for those phenomena obtained from experiments in the past century [78–80]. These numerical methods have been widely used for simulating multiphase flow in microchannels, capillary filling, surface wettability, solid-liquid interface slip, liquid flow in porous media, and so on [81].

The flow states of the fluid are typically gaseous, liquid, and multiphase. The most popular numerical calculation methods used from the macroscopic point of view are CFD [7], such as the finite element, finite volume, and finite difference methods. These methods are based on the continuous medium model of the fluid, ignoring microscopic interactions. Then, the Navier–Stokes equation is solved to obtain the state of motion of the

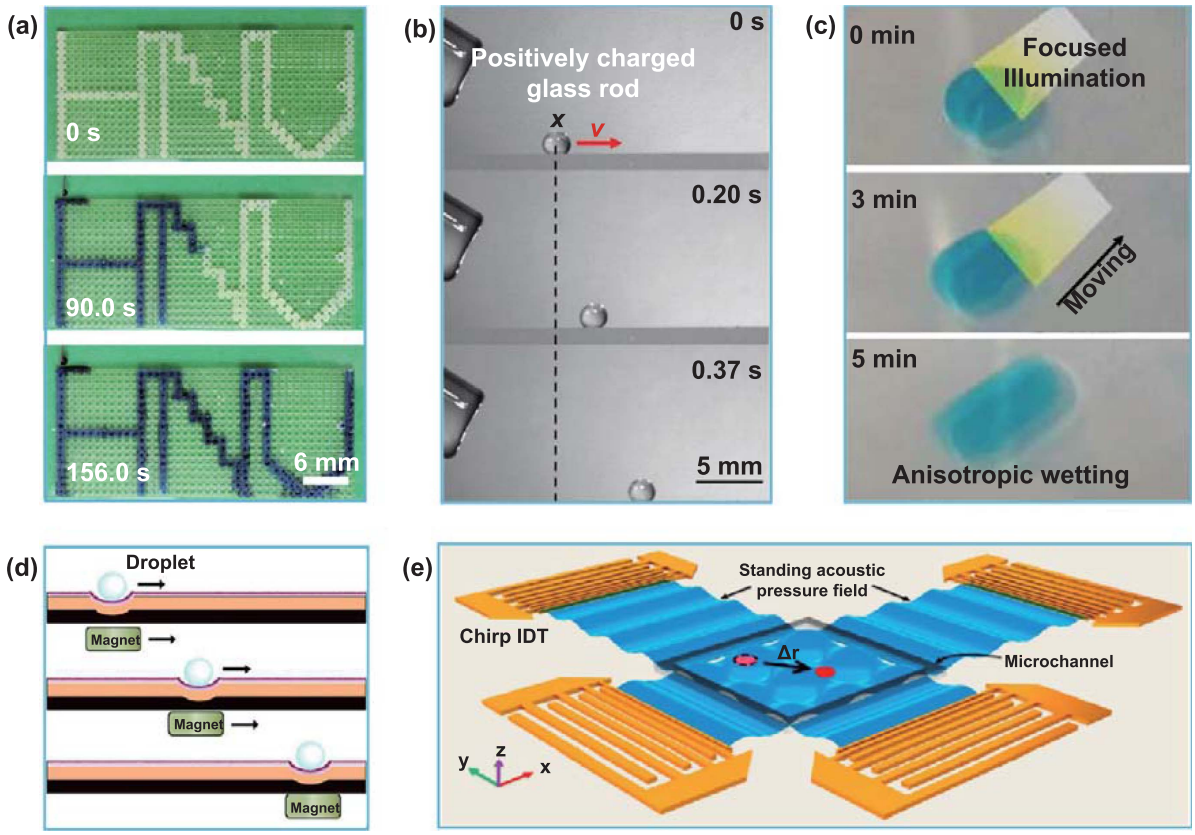

Figure 5. Functional microfluidic devices with different driving forces. (a) Capillary force for transporting liquids [69]. [69] John Wiley & Sons. [© 2023 Wiley-VCH GmbH]. (b) Electrostatic force for manipulating liquid to achieve high-speed motion [72]. [72] John Wiley & Sons. [© 2019 WILEY-VCH Verlag GmbH & Co. KGaA, Weinheim]. (c) Blue light induced droplet motion [74]. Reproduced from [74]. CC BY 4.0. (d) Schematic of droplet manipulation by magnetic force [75]. Reproduced from [75] with permission from the Royal Society of Chemistry. (e) Manipulation of cells in fluids by varying sound field frequency [76]. Reprinted from [76], Crown Copyright © 2016 Published by Elsevier B.V. All rights reserved.

fluid. However, these macroscopic approaches never consider surface wettability effects.

The numerical calculation technique used from the microscopic perspective of the fluids which can consider surface wettability effects is the MD method [8] and the LBM [9]. The MD method is based on the Newtonian classical mechanics for modeling the physical trajectories and states of atoms/molecules [79]. Thus, the results obtained from MD simulation method can provide a more detailed description of the conformational space, equilibrium properties, dynamics of molecules, and statistical properties. Unfortunately, even a simple question calculated by MD method requiring an overly long simulation time is a critical drawback for such a method. Moreover, because the chemical bonds among molecules or atoms are established in MD simulations, they cannot be broken or created during chemisorption, chemical reactions. Also, the time and scale of the MD simulations are relatively microscopic, typically below 10 ns at scales below 10 nm [84]. Based on MD method, Martic *et al* [85] investigated capillary flow processes applying Washburn equations to characterize the properties of porous media and obtained a more satisfactory fit. Koplik *et al* [86] studied the low-Reynolds-number Poiseuille flow and kinematic contact lines using MD method.

The LBM is a CFD method at the mesoscopic scale [9], which is now widely used to describe multiphase flow and phase-change heat transfer problems in which wettability effects play a key role [87]. The LBM is simple and efficient in describing fluid interaction. It can be easily used to set boundary conditions of complex geometries and different wetting conditions, and is well adapted to multiphase flow and multicomponent problems. It is also highly parallelizable. However, the key drawback of this method is instability under certain conditions [88]. In 1996, Chen *et al* [89] proposed simple extrapolation to simulate the capillary fluid flow and 2D Poiseuille flow with LB method. In 1997, Spaid and Phelan [90] improved the traditional LBM to solve the microscale flow in fibrous porous media. In 2006, van der Graaf *et al* [91] investigated the process of droplet formation in individual pores of T-shaped microchannels.

The DSMC is also used for the numerical study of microfluidics, which is a direct particle simulation method based on kinetic theory [10]. The DSMC is highly applicable to the solution of flow problems with high Knudsen number [92], which is quite suitable for the commonly high Knudsen number flow of gases in microchannels [93]. Compared with those other methods, the runtime and storage requirements are

Table 1. The comparison of advantages and disadvantages of different simulation methods for microfluidics.

Simulation methods	Key theories or ideas	Calculation scale	Advantages	Disadvantages	References
Finite element method (FEM)	Finite number of non-overlapping elements	Macro continuous media	Good conservativeness	Difficulty in handling complex equations	[82]
Finite volume method (FVM)	Finite number of cell volumes (computational domain)	Macro continuous media	Good grid adaptability Better conservativeness Flexibility	Relatively not very high precision	[78]
Finite difference method (FDM)	Differential approximation of each order derivative	Macro continuous media	Simple and mature high precision	Difficulty in handling complex meshes	[83]
Molecular dynamic (MD)	Newton mechanics	Microscopic particles	Absence of random factors and ability to simulate the fundamental processes associated with the path of atomic motion	Large calculation volume cannot describe chemical reactions	[79]
Lattice Boltzmann method (LBM)	Lattice gas automaton	Mesoscopic model	Simple and efficient, able to solve multi-phase flow and multi-component problems	Higher memory requirements	[9]
Direct simulation Monte Carlo (DSMC)	Kinetic theory probabilistic models	Mesoscopic model	High calculation accuracy for dilute gas flows	More calculated steps	[80]

the two major limitations of DSMC simulation method [94]. In addition, there are numerical and statistical errors for the DSMC method because its computational results are determined by the sample size and averaging process, and the solution must be quantified to verify the accuracy of results [95]. In the past, the DSMC method was mainly applied to thin-atmosphere dynamic problems [96]. In 2003, Wang and Li [97] used DSMC to study the non-ideal gas flow and heat transfer in micro/nanochannels. In 2004, Wang and Li [98] simulated microgas flow in micro-electro-mechanical system (MEMS) devices using a modified DSMC method, and the geometry of the microchannels significantly affected the flow performance inside them. In 2016, Kawagoe *et al* [99] used the DSMC method to simulate the pressure-driven gas flow through porous media. The results show that Darcy's law can be applied to porous media with micro/nanopores, which open the gate for theoretical study of such kind of structures.

3. Materials and fabrication methods for functional microfluidic devices

The applications of functional microfluidic devices are severely limited by the fabrication methods [100, 101]. State-of-the-art fabrication methods used in the semiconductor industry decrease the minimum characteristic sizes of microchannels down to several micrometers. However, the enormous initial investment and extreme-high operational fee are unacceptable. Moreover, ensuring that the facility can provide patterns with feature sizes matching the critical dimension required by microfluidic devices is critical [102]. Therefore, adopting other available fabrication methods with various resolutions to manufacture functional microfluidic devices [103, 104] is necessary. After the first transistor being invented by the team of Shockley in 1947, many advanced fabrication techniques, including CO_2 lasers [105, 106], femtosecond lasers [107–109], imprinting methods [14], molding [110, 111], sintering [24, 112], etching [113–115], lithographic fabrication [116, 117], 3D printing techniques [41, 118–124], etc. have been well developed and applied to the manufacture of functional microfluidic devices (figure 6 and table 2).

3.1. Materials for different types of microfluidic devices

The essential properties of microfluidic devices include processing characteristics, durability, hardness, transparency, biocompatibility, and thermostability [126]. Meanwhile, there are more and more microstructures which have been added into microchannels, including pillars, sawteeth, mushroom heads, and so on [134]. Thus, the selection of optimal materials satisfying these requirements needs to be the priority before the fabrication of microfluidic devices, including polymers [14, 102, 117, 128], metals [135], glass [105, 114, 136], silicon [114, 136], and ceramics [137]. Among which, polymers, including PDMS [102, 126, 138–141], PMMA [14, 128, 142–145], epoxy resins [15], hydrogels [110, 146, 147], etc [19], are increasingly used for microfluidic devices because of their merits of low cost and outstanding formability [126].

PDMS is one of the most widely used materials for microfluidic devices [126] with the merits of high elasticity, low viscosity variation with temperature, water resistance,

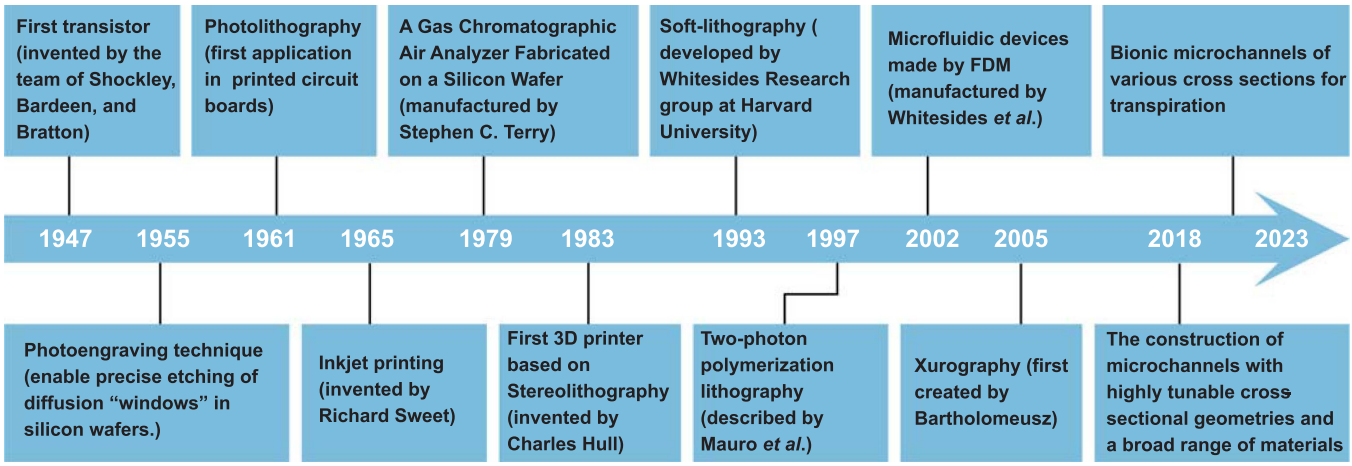

Figure 6. Significant benchmarks in the progress of functional microfluidic device fabrication methods. Based on information from the references [125–127].

Table 2. The characteristics of various fabrication methods.

Method	Approximate resolution	Starting material requirements	Low costs
Laser method	15 μm [105, 106]	Polymer [128], silica [129]	Negative
Molding method	100 μm [110, 111]	Polymer [130], hydrogel [110]	Positive
Imprinting method	20 nm [14]	Polymer [14]	Positive
Lithography method	20 μm [116, 117]	Polymer [117]	Negative
Etching method	5 μm [113–115]	Glass [114], polycrystalline diamond [115]	Negative
Fused deposition modeling (FDM)	100 μm [120, 131]	Thermoplastic polymer (filament)	Positive
Polyjet or multi-jet modeling (MJM)	50 μm [121]	Low viscosity ink $V_{app} < 0.25$ Pas [121]	Positive
Digital light processing (DLP)	10 μm [41, 122, 132]	Photosensitive resin [41], Hydrogel [133]	Negative
Two-photon polymerization (TPP)	50 nm [119, 123]	Photoresist [123], Sol-gel [119]	Negative

small surface tension, weather resistance, high shear resistance, low cost, well-operated mold, excellent clarity, natural hydrophobicity, biological compatibility [111], and electrical insulation [102]. Thus, various microfluidic devices made of PDMS have been well developed, including topologically complex 3D microfluidic devices [138], hydrophilic PDMS devices treated with oxygen plasma [139], glass coated PDMS microfluidic channels for generating emulsion [140], microfluidic devices with electronic components [141], and so on. However, the weakness of PMDS is also intolerable to researchers [148], including extreme high air permeability [149], long curing time [126], and instability when subjected to hydrophilic treatment [150].

Another primarily used material for biomedical microfluidic devices is PMMA [126]. It is an amorphous thermoplastic [142] owning attractive mechanical and chemical properties, considerable toughness, excellent insulativity, outstanding weather resistance, satisfactory processing characteristics, and excellent compatibility [128, 133, 151]. In addition, the transparent PMMA enables light of various wavelengths to pass through [14] with unique aging resistance [14]. Thus, PMMA has been extensively applied to microfluidic devices, including pressure-driven 3D microfluidic chips with multiple logic Boolean functions [143], PMMA optical detection chips [144], pneumatic microvalves and micropumps [145]. However, PMMA is easily scratched because of its extremely low elastic modulus [126].

Resins are also utilized to manufacture microfluidic devices [41, 69, 152, 153] because of their excellent mechanical properties, chemical stability, high/low-temperature resistance, low shrinkage rate, low cost, etc [15]. The resins are mainly composed of polymer monomers and prepolymer into which a light initiator is added. Under the action of a certain ultraviolet (UV) light (250–405 nm), polymerization reaction inside resins occurs, conversing them from liquid to solid, forming the designed complex 3D structures [154]. Functional microfluidic devices made of resins have been applied to underwater anaerobic chemical reactions [155], bionic open microchannels for transpiration [156], cellular fluidics [69], bending tubes with peristome-mimetic structures for controlling water elevation [157], and so on [158, 159].

Hydrogels are hydrophilic 3D network structured gels that rapidly expand in water and absorb a lot of water without dissolving in the swelling state [133, 160].

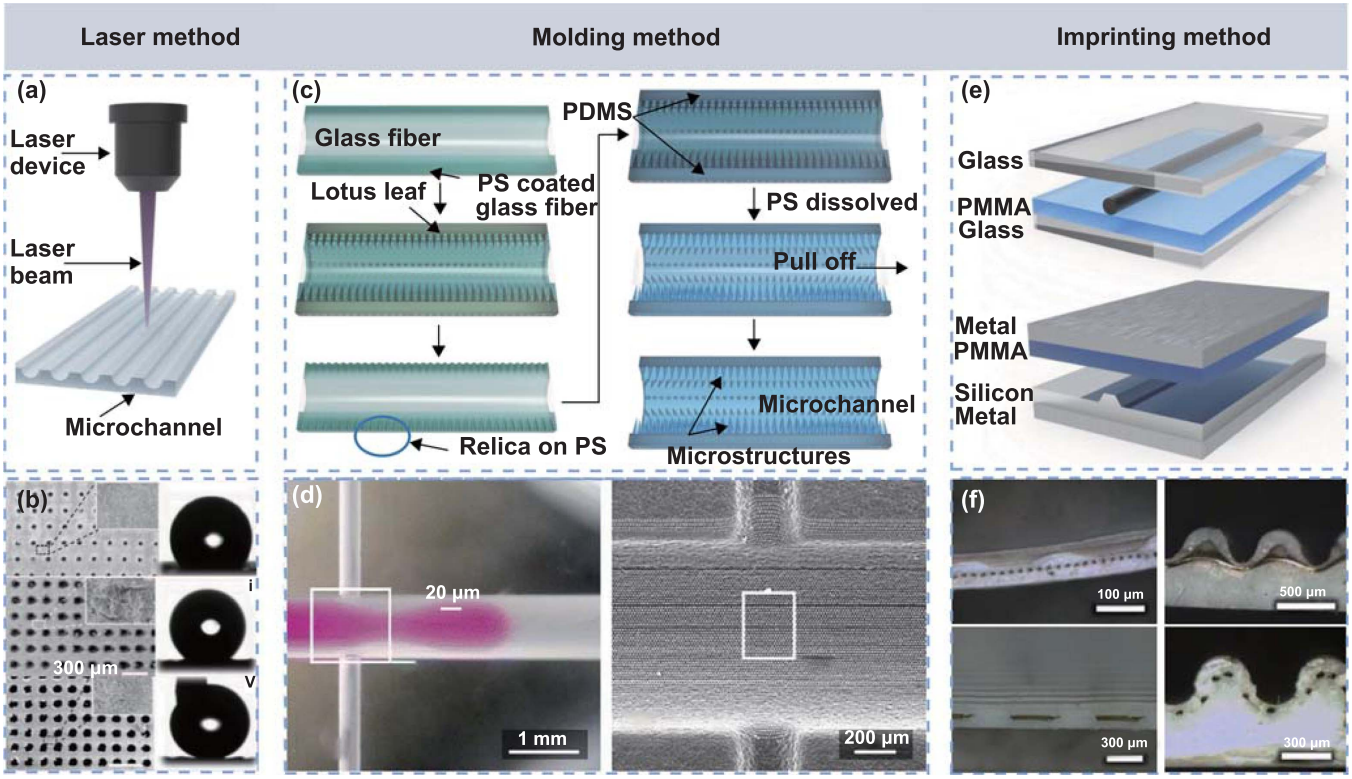

Figure 7. Traditional fabrication methods for functional microfluidic devices. (a) Schematic of functional microfluidic devices fabricated by using lasers. (b) Janus microhole-arrayed polydimethylsiloxane fabricated by a one-step femtosecond laser [177]. [177] John Wiley & Sons. [© 2019 WILEY-VCH Verlag GmbH & Co. KGaA, Weinheim]. (c) Schematic of functional microfluidic devices fabricated by using molding methods. (d) Cylindrical superhydrophobic microchannels fabricated by replicating lotus leaf structures on internal walls [178]. Reproduced from [178]. CC BY 4.0. (e) Schematic of functional microfluidic devices fabricated by using imprinting methods. (f) Functional microfluidic devices with more complicated structures manufactured by imprinting thermoplastic substrate with silicon wafer [179]. Reproduced from [179] with permission from the Royal Society of Chemistry.

Water-soluble or hydrophilic polymers can form hydrogels via chemical/physical crosslinking [161]. The advantages of hydrogels including biocompatibility, degradability, and permeability enable them extensive applications as functional microfluidic chips [162, 163], 3D bioprinted functional tissues [164], generation and separation of droplets through immiscible multiphase flows inside microchannels [101], bioinspired solar evaporators [158], and so on [165].

3.2. *Traditional fabrication methods for microfluidic devices*

3.2.1. Laser methods. The process of microfluidic devices fabrication by laser is a complicated combination of photothermal and photochemical actions [166, 167]. Some chemical bonds in the workpiece burst directly during photon absorption process, while the others will be thermally burst due to the heat released by excited molecules [168–170]. Such a process is dominated by the frequency and wavelength of laser beam [171]. Infrared radiation with a wavelength of 10.6 μm is commonly employed for such a method [105]. The temperature of workpiece rapidly increases wherever the continuous CO_2 laser beam is focused on it. Consequently, the material melts and disintegrates to form microchannels (figure 7(a)). The strength of chemical bonds and structures of materials are crucial to the decomposition process. For example, as one of the most used materials for fabricating microfluidic devices, PMMA [172] vaporizes in the form of monomers producing microchannels when the temperature considerably exceeds its melting point. In contrast, femtosecond lasers [108, 173, 174] typically own a wavelength of 1030 nm, pulse width of 250 fs, frequency of 100 kHz, and focal point of 5 μm. Such a method has an advantage over traditional lasers in fabricating transparent capillary tubes with micro/nanopatterns on internal surfaces [128]. In particular, the micro/nano-grooves in the axial direction have an active influence on capillary rise [175, 176], such as a Janus membrane for bubble unidirectional transportation underwater (figure 7(b)) [177].

3.2.2. Molding methods. As a traditional method, the molding method is one of the most convenient and cheap approaches to manufacture functional microfluidic devices [111], which fundamentally leverages the viscoelasticity, optical transparency, biological compatibility, durability [180, 181], and biodegradability [182, 183]. First, a gel wire is used to determine the geometric parameters of the microfluidic devices, which have been prepared and cured using an aqueous solution of glycerol and agarose in a glass microchannel. Then, the gel wire is arranged in the desired pattern on a film of precured PDMS in a dish covered by another layer of PDMS, which will be cured below the melting point temperature of

agarose. Finally, the PDMS microchannels are formed after removing the original gel wires using boiling water and hydrophobic treatment (figure 7(c)). The two major problems during the fabrication of the negative replica are the formation of small pores induced by spontaneous de-wetting and discontinuous seam (figure 7(d)) [178].

3.2.3. Imprinting methods. Imprinting methods are simple, convenient, and low-cost for fabrication of functional microfluidic devices [184, 185]. They obviate the indispensability of the thermoplastic substrate during the stamping process and improve the production efficiency to more than 100 samples per template. The repeatability of imprinting methods is extremely high that the difference of the imprinted microchannels is less than 1% before and after dozens of imprints [14]. A small wire is impressed on a plastic substrate softened by heating for the first-generation imprinting technique [186]. In contrast, the second-generation imprinting technique involves the manufacture of functional microfluidic devices with more complicated structures by imprinting a thermoplastic substrate with a silicon wafer (figure 7(e)) [14]. In addition, other silicon etching process and materials can be used to fabricate microchannels with high aspect ratios [14]. They can overcome problems caused by the anisotropic etching angle, which makes a big difference on the feature size of functional microfluidic devices [126]. Finally, an open microchannel can not only attach to other microchannels but also serve as a flexible and adhesive polyfilm to seal the microchannels [14]. More importantly, the length and inner diameter of microchannels can be conveniently regulated to obtain the best microfluidic performance (figure 7(f)) [179].

3.3. Lithography and etching

With the rapid development of functional microfluidic systems, the methods to fabricate microfluidic devices with more complex 3D geometries, smaller feature sizes, and larger sample widths are in urgent need [187]. Thus, lithography and etching techniques have been proposed and developed by researchers for manufacturing complex functional microfluidic devices even at the submicron-scale [188].

3.3.1. Lithography. Lithography can be used to manufacture functional microfluidic devices with extremely high precision (figure 8(a)) [189]. First, a layer of uniform photoresist is deposited on a silicon dioxide (SiO_2) wafer. Then, a mask is used to expose and cure the photoresist and form a cured geometric figure completely corresponding to the mask on the photoresist layer. A pattern corresponding to the mask on the photoresist is developed, which causes the SiO_2 wafer to resist the etching process. A wafer shape corresponding to the photoresist pattern is etched into the SiO_2 using various light sources. Finally, the photoresist layer is peeled off, and an upper cladding layer is deposited onto the already formed wafer layer pattern. The feature sizes of the microchannels depend on the wavelength of the light sources in the exposure system.

To date, many light sources, such as UV, deep UV, x-rays, silicon–oxide–nitride–silicon [116], are available. One of the advantages of lithography is that it can precisely control the shape and size of the patterns [190]. In addition, it can generate contours on the entire chip's surface. However, as the main disadvantage of lithography, it must be used on flat surfaces under extremely clean conditions. Also, it is less effective when used on uneven surfaces. Currently, an inexpensive and convenient approach to manufacture microchannels is combining soft lithography and molding methods [148]. First, a 30 μm-thick initial mold of the SU-8 layer determining the shape of the final microchannels is created by photolithography. Then, the liquid PDMS prepolymer is poured onto the mold to obtain the same structure as the initial SU-8 layer after complete curing at 65 °C for 2 h. The bottom plane of the microchannels, manufactured by the spin costing method with the support of oxygen plasma activation, is bonded to the PDMS microchannel layer (figure 8(a)). Owing to the excellent elasticity of the materials, the PDMS functional microfluidic devices exhibit a considerable capability of flexibility. Moreover, such a straightforward and low-cost fabrication process can create functional microfluidic devices with complex topologies and diameters ranging in 25–150 μm for various biomedical applications (figure 8(b)) [149].

3.3.2. Etching method. Etching, a technology of pattern processing associated with lithography, is a process of removing undesired materials from a silicon wafer using chemical/physical methods [191]. Wet etching and dry etching are two simple and typically used etching techniques. Wet etching uses solvents/solutions for etching [192], which is a purely chemical reaction process [193]. Accordingly, a solution and pre-etching materials are used to remove the parts that are not masked by the film materials. It has the advantages of satisfactory selectivity, excellent repeatability, high production efficiency, simplicity in terms of equipment and low cost [114]. Its disadvantages are the necessity for considerable drilling, inadequate control over graphics, and waste of considerable amounts of chemicals [194, 195]. In contrast, there are various dry etching methods, including light volatilization, vapor-phase etching, plasma etching, metal etching, dielectric etching, silicon etching [196], and so on. There are several advantages of dry etching methods for fabrication of microfluidic devices, such as repeatability, acceptable anisotropy, controllability, high selection ratio, flexibility, and easy automation [136]. Moreover, they are clean without producing chemical waste or introducing pollution during the treatment process [136]. However, dry etching is costly and requires complicated equipment [197].

An efficient, low-cost, and distinct method for manufacturing functional microfluidic devices involves combination of etching and thermal blowing [114]. Square microchannels with a depth of 30 μm can be patterned on a silicon wafer with photoresist using deep reactive ion etching. Applying anodic bonding, a 500 μm-thick glass is irreversibly bonded with a silicon wafer at 410 °C and 1 atm in a nitrogen environment. Because the softening point of glass is around

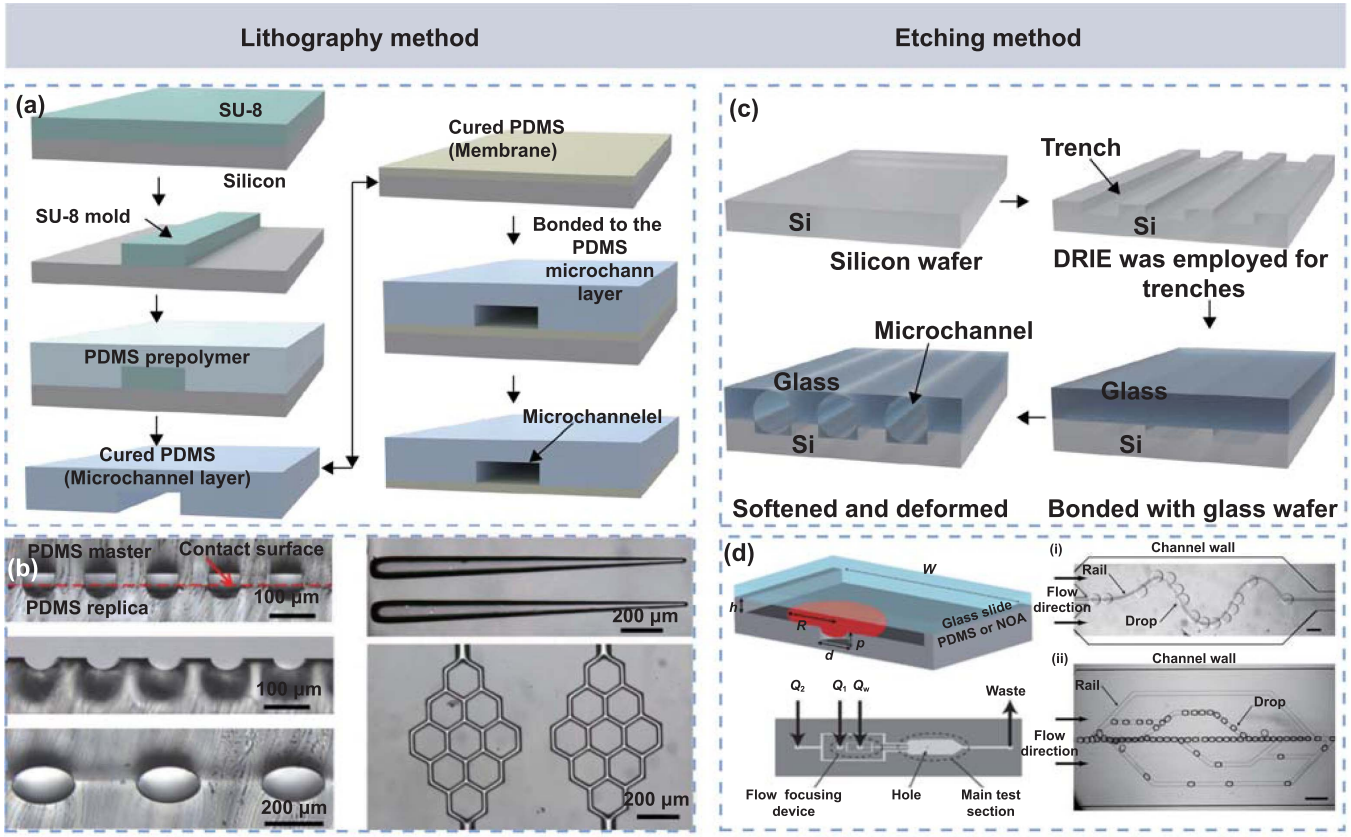

Figure 8. Lithography and etching methods for the fabrication of functional microfluidic devices. (a) Schematic of functional microfluidic devices fabricated based on lithography methods. (b) Lithography methods can be easily applied to manufacture circular microchannels with a wide range of diameters from 25 μm to 150 μm [149]. Reprinted from [149], © 2016 Elsevier B.V. All rights reserved. (c) Schematic of functional microfluidic devices fabricated based on etching methods [113]. (d) Functional microfluidic devices manufactured by etching methods [113]. Reproduced from [113] with permission from the Royal Society of Chemistry.

820 °C, the sample must be annealed at a temperature around 820 °C–950 °C for 2 h. The glass behaves as a Newtonian fluid above the softening point and is deformed by trapped air (like glass blowing), forming cylindrical microchannels during bonding. Finally, the samples with different shapes and feature sizes (fabricated without any chemical foaming agents or pollutants) must be cooled gradually to keep them transparent and free from crazing (figure 8(c)). Depending on the annealing temperature, circular microchannels with a diameter ranging from 20 μm to 75 μm have been fabricated by such a method [113] (figure 8(d)). Furthermore, a method for nanochannels' fabrication via the galvanic corrosion of coupled metals has also been previously reported [198].

3.4. 3D printing methods

To date, there are many different types of 3D printing techniques including inkjet [199], selective laser sintering/melting [24, 200], fused deposition modeling (FDM) [201], direct ink writing [202, 203], SLA [154], digital light processing (DLP) [15], and two-photon polymerization (TPP) [204, 205], which differ in the operating principles, depositing manner of layers, and the applied materials [126]. Recently, 3D printing techniques have been widely used for fabrication of various functional devices [206–208], including functional microfluidic devices [155].

3.4.1. Fused deposition modeling (FDM). As one of the most widely used 3D printing technology, FDM is an additive manufacturing process belonging to the material extrusion family (figure 9(a)) [209]. The material used for such a method is thermoplastic polymer in the form of filaments, which are fused at temperatures ranging from 190 °C to 230 °C. The filaments are selectively squeezed out through the nozzle with a circular hole of 200 μm on the platform to build objects layer by layer in a predetermined path. The distance between the nozzle and platform, extraction speed of the material, and relative moving speeds of the nozzle and platform are the primary parameters influencing the feature sizes and shape of printed objects. The FDM technology is typically used to fabricate functional microfluidic devices with molding methods [150]. A sacrificial microchannel mold is firstly manufactured with a polyvinyl alcohol (PVA) filament and then removed from the printing platform, which determines the shapes of the microchannels. The microchannel mold is placed on a thin cured polymer layer and covered with a fully degassed uncured

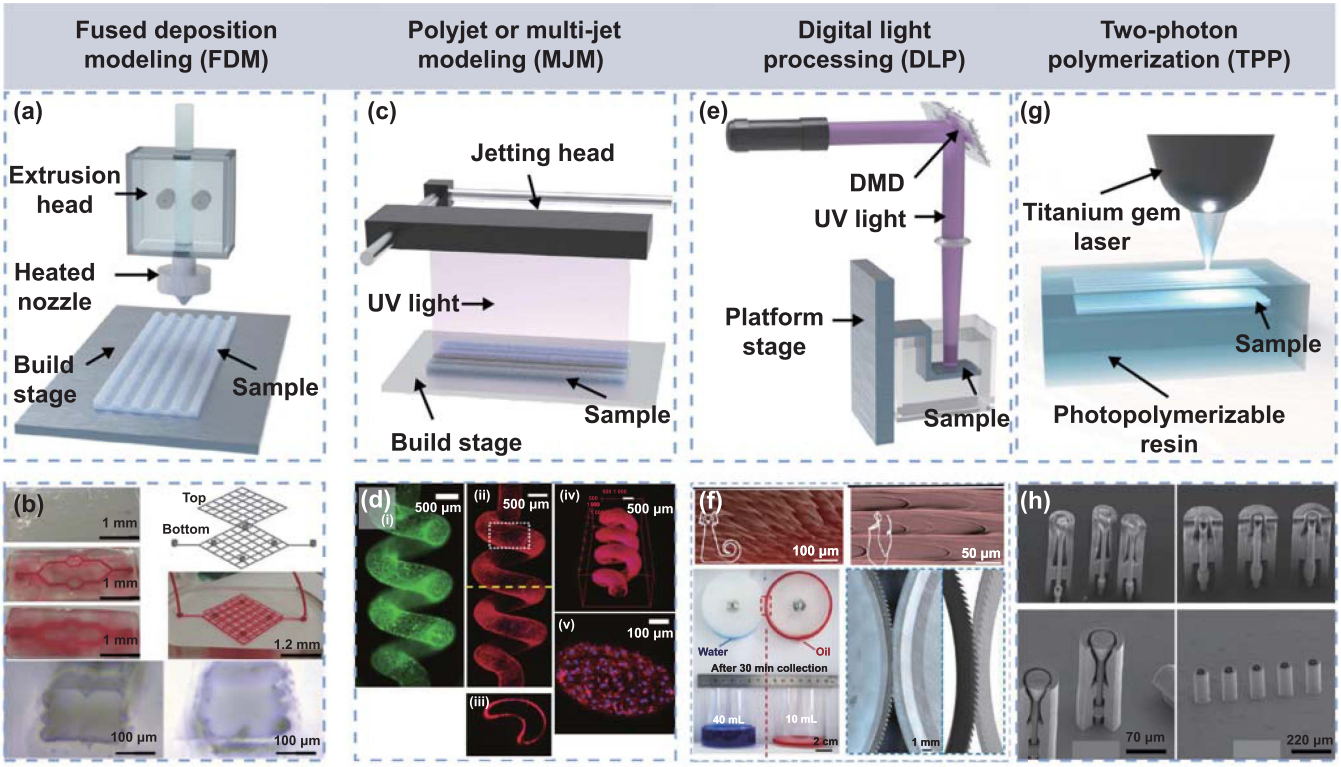

Figure 9. 3D printing methods for fabrication of functional microfluidic devices. (a) FDM technology is typically used to fabricate functional microfluidic devices with thermoplastic polymer [209]. (b) Sacrificial molding method based on FDM for fabrication of functional microfluidic devices [201]. [201] John Wiley & Sons. © 2018 WILEY-VCH Verlag GmbH & Co. KGaA, Weinheim. (c) Photopolymer is jetted through linearly arranged nozzles in a continuous or drop-on-demand mode, sprayed onto the platform in a form of microdroplets, and finally cured with an even UV light source to form functional microfluidic devices [210, 211]. (d) Spiral microchannels [199]. [199] John Wiley & Sons. © 2018 WILEY-VCH Verlag GmbH & Co. KGaA, Weinheim. (e) Single-photon polymerization (SPP) process repeatedly occurs on the surface of photosensitive resin where the UV light irradiates to fabricate microfluidic devices [212]. (f) 3D capillary ratchet-induced liquid directional steering [213]. Reproduced from [213]. CC BY 4.0. (g) Focal point moves over the photosensitive area to solidify the material with the two-photon absorption effect [214]. (h) A printed complex microscale check valve [215]. Reproduced from [215], with permission from Springer Nature.

polymer. An intact microchannel is obtained after ultrasonic cleaning in a water bath and eliminating the printed PVA mold. Furthermore, sacrificial molding based on FDM for fabrication of microchannels within biomimetic matrix can be potentially applied in tissue engineering (figure 9(b)) [201].

3.4.2. Polyjet/multijet modeling (MJM). MJM exhibits high resolution and incomparable compatibility with various materials having a wide range of features (e.g. hardness, flexibility, long-range elasticity, and multiple colors [210]) numbering more than 100 [216]. However, the materials are expensive and exclusive. The photopolymer is jetted through linearly arranged nozzles in continuous or drop-on-demand mode, sprayed onto the platform in the form of microdroplets, and finally cured with an even UV light source. The water-soluble holder, which is completely removed after finishing the printing, is added under a high cantilever structure during processing. Depending on the feature sizes of the functional microfluidic devices, the water-soluble holder must be soaked in water for a period ranging from 1 h to 6 h, which is followed by ultrasonic cleaning in 2% NaOH solution for 1–3 d (figure 9(c)).

For a roller texture direction similar to that of the microchannels, the 3D printer orientation must be aligned with the nozzles [199]. The smallest feature size of the printed microchannels is approximately 200 μm. Based on polyjet modeling, the same coaxial nozzle method was reused by Gao *et al* [161]. Once the sodium alginate solution and calcium chloride solution come into contact, Ca^{2+} diffuses into the sodium alginate solution and begins to crosslink, producing a calcium alginate filament with hollow microchannels. In addition, hollow microchannels with inner gelled alginate and outer ungelled alginate can be manufactured by regulating the concentration and flow rate. Finally, by printing on the previous layer via the vertical movement of the z platform, the desired microchannels will be obtained [217]. After confirming the printability and stabilization of the hydrogels, spiral microchannels can be prepared to mimic the blood vessels (figure 9(d)).

3.4.3. Digital light processing (DLP). As one of the most popular 3D printing techniques, DLP printers project the image signal after digital processing [158, 218], which is based on the digital micromirror devices (DMDs) for achieving the

Table 3. Summary of advantages and disadvantages for functional microfluidic devices fabrication methods.

Method	Advantages	Disadvantages	Main area of applications
Laser method	Very low fabrication time, fit for mass production	High power consumption, tough to maintain, high initial investment cost	Chemical applications [221], mechanical and electronic heat sink [222]
Molding method	Fabrication of small structures, high cost, effective	Low strength, presence of weld lines	Electrochemistry [223], cell trapping [224] and DNA elongation [225]
Imprinting method	Tailored to individual needs	High roughness, high temperature	Biomechanical [226] and chemical applications [227]
Lithography method	High aspect ratio, complex topography	High environmental requirements	DNA analysis [228], blood [229], protein synthesis [230], chemistry [228]
Etching method	Smooth surface, no burrs, high production rate	Non-parallel walls, selective material removal	Electrochemistry [231], biomechanics [232]
Fused deposition modeling (FDM)	Low cost, suitable for large prints	Low resolution, poor surface quality	Microfluidic devices [233], sensors [234]
Polyjet or multi-jet modeling (MJM)	High precision, high resolution	High cost, low printing speed	Biochips [235], microfluidic devices [236]
Digital light processing (DLP)	High-speed, high resolution, high surface quality, complex structures	High cost, relatively few material options	Bionic structures [69, 155], seawater desalination [158]
Two-photon polymerization (TPP)	Fabrication of nanostructures, high-speed	Extremely expensive, few material options	Microrobots [237], biomedical engineering [238]

visual digital information display [212, 219]. The precision of the functional microfluidic devices is determined by the projected DMD pixel size and the optical system, which is currently as small as 500 nm. Every 2D slice from the 3D functional microfluidic devices is projected onto the platform through a release liner in the form of UV light (405 nm). The light curing process occurs on the top of the photosensitive resin where UV light irradiates. This operation process is repeated after the longitudinal shift of the platform driven by a high precise stepper motor (figure 9(e)). The functional microfluidic devices are removed from the platform and cleaned in isopropanol using an ultrasonic machine. Finally, the uncured resin and isopropanol are removed from the functional microfluidic devices using compressed N_2 air [41]. Currently, the spectral response features of liquid resin, DMD feature size, and z-axis resolution limit the precision of DLP technology [158]. As a recently reported bionic microfluidic system, a dual-bionic superwetting gears system achieves high separation efficiency of oil and water by utilizing surface wettability and precisely printed topological microstructures (figure 9(f)) [213].

3.4.4. Two-photon polymerization (2PP). Consequently, the 3D printing of low-roughness and high-precision devices (such as optical components and nano-structural devices [214]) is difficult to implement. Two-photon polymerization (2PP) is expected to solve the problems of limited fabrication precision. Normally, owing to the linear relationship between matter and light, the transmittance and absorption rates for a specific wavelength of matter are definite and do not vary with the change in light intensity. However, two-photon absorption is a third-order nonlinear effect [118]. That is, the effect increases as the optical energy density increases. Compared with SPP, which utilizes one photon as the base unit for light curing (used by SLA, DLP, and MJM), the 2PP utilizes two photons as the base unit for light curing under extremely harsh conditions that require specific substances and extremely high energy density. Sufficient irradiance for ensuring the simultaneous absorption of two photons is observed only at the center of the highly focused laser. The two-photon absorption effect only occurs when the light intensity reaches a certain threshold value. If the laser is focused, the polymerization reaction area can be limited to a small area near the focal point. The focal point moves in the photosensitive material using a nanoscale precision stepper motor. The photosensitive material solidifies at the position where the focal point passes (figure 9(g)) [220]. A complex shape readily assembled microscale check valve can be fabricated based on such an advancing method, which exhibited good dimensional accuracy (figure 9(h)) [215].

In summary, researchers have extensively studied various fabrication techniques with certain materials to precisely manufacture functional microfluidic devices (table 3). Different fabrication methods own unique advantages, disadvantages and processing properties, so it is particularly important to choose a processing method that best meets their own needs and application prospects.

4. Design and applications of functional microfluidic devices

From the foregoing discussion, there are numerous merits of functional microfluidic devices, such as compactness, microscale, and ease of integration [26]. These advantages

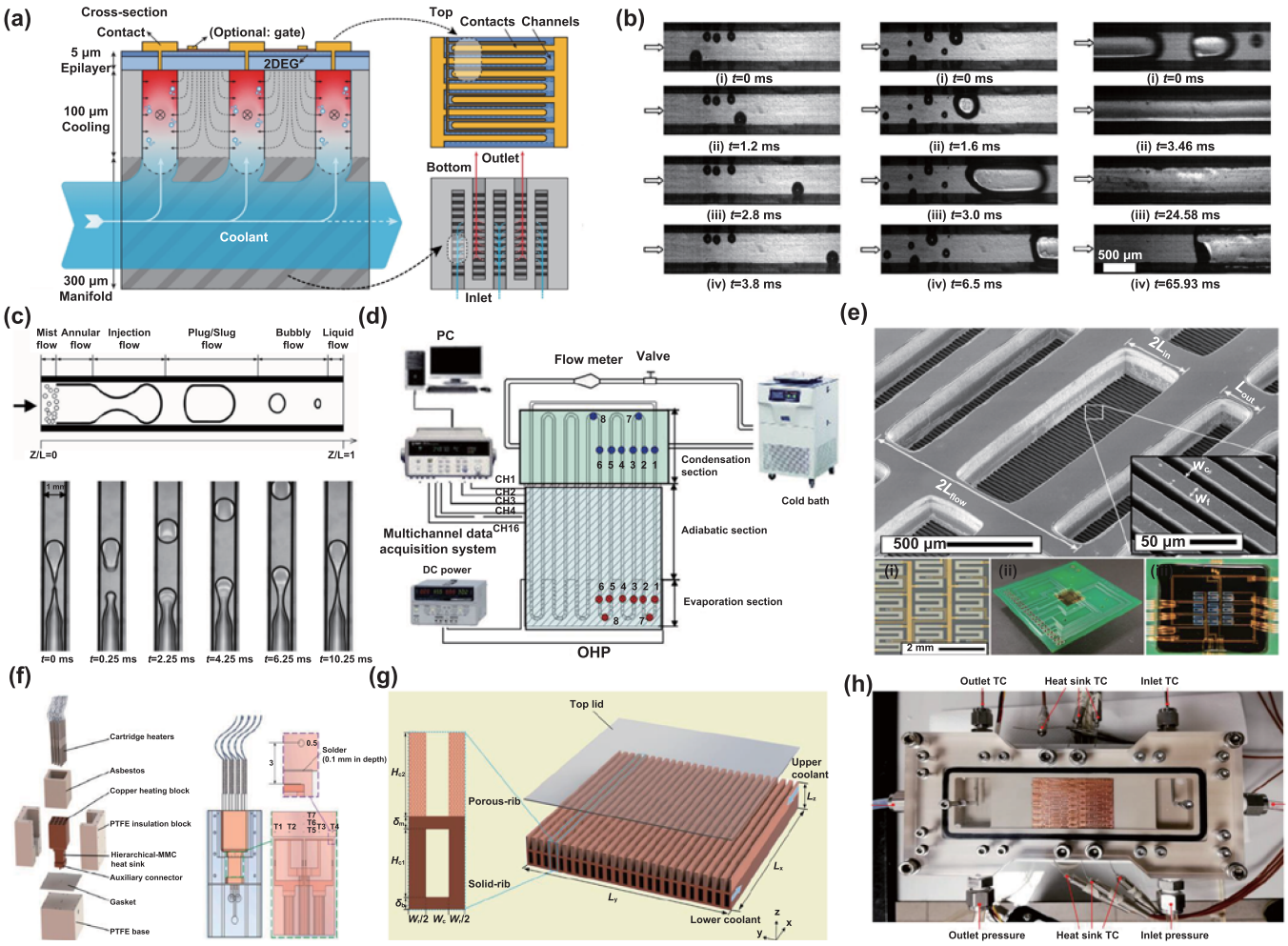

Figure 10. Various microfluidic heat sinks. (a) Co-designed microfluidic cooled electric devices [241]. Reproduced from [241], with permission from Springer Nature. (b) Effects of inlet/outlet configurations on flow boiling instability in parallel microchannels [242]. Reprinted from [242], Copyright © 2007 Elsevier Ltd. All rights reserved. (c) The condensation of steam in microchannels [243]. Reprinted from [243], Copyright © 2007 Elsevier Ltd. All rights reserved. (d) Thermal performance of an oscillating heat pipes with Al_2O_3 nanofluids [244]. Reprinted from [244], Copyright © 2009 Elsevier Ltd. All rights reserved. (e) Hierarchical manifold microchannel heat sinks for high-heat-flux two-phase cooling of electronics [245]. Reprinted from [245], © 2017 Elsevier Ltd. All rights reserved. (f) Hierarchical manifold microfluidic heat sinks with uniform flow distribution [246]. Reprinted from [246], © 2021 Elsevier Ltd. All rights reserved. (g) Double-layered microfluidic heat sinks with semi-porous ribs by multi-objective genetic algorithm [247]. Reprinted from [247], © 2019 Elsevier Ltd. All rights reserved. (h) An actual apparatus of microfluidic heat sink [248]. Reprinted from [248], © 2019 Elsevier Ltd. All rights reserved.

of functional microfluidic devices have played an influential role in many promising applications, such as heat sinks, mass transfer, chemical reactions, detection, and biomedical engineering.

4.1. Heat sink

Microfluidic heat sinks own small size with ultra-high heat transfer coefficients [239], thus, various microfluidic heat sinks with marvelous heat transfer performance have been developed in the past 40 years [27]. Moreover, they demonstrate excellent pressure resistance, which can be widely utilized in aerospace, chemical engineering, industrial manufacturing, and many other fields [240]. Recently, van Erp *et al* [241] proposed co-designing electronics with sustainable microfluidic cooling capability (figure 10(a)), which integrates electronics and microfluidics for efficient cooling of extreme heat flux extraction. Wang *et al* [242] investigated the effect of inlet/outlet configuration on flow boiling instabilities in parallel microchannels (figure 10(b)), and the flow boiling instabilities in parallel microchannels with three types of connections are compared. Quan *et al* [243] further experimentally studied the injection flow during condensation in microchannels (figure 10(c)). The flow pattern maps in terms of heat transfer rate versus mass flux for the annular flow regime and slug-bubbly flow regime in microchannels are proposed. Besides, Qu *et al* [244] also reported the thermal performance of an oscillating heat pipe with water based Al_2O_3 nanofluids under different mass fractions and filling ratios (figure 10(d)), which decreased the thermal resistance with a minimum of 0.14 $°C \cdot W^{-1}$ (or 32.5%) when compared with that of the pure water.

Subsequently, Drummond *et al* [245] proposed a 3 × 3 array of microfluidic heat sinks (figure 10(e)), which can remove high heat flux (910 $W{\cdot}cm^{-2}$) with a pressure drop and a temperature of 162 kPa and 47 °C, respectively. Zhou *et al* [246] demonstrated a novel manifold microfluidic heat sink with a stacked configuration (figure 10(f)), which can mitigate flow maldistribution by optimizing the flow path. The overall thermal resistance is reduced by 7%–13% with a volumetric flow rate of 0.12–1.17 $l{\cdot}min^{-1}$. Wang *et al* [247] proposed a porous medium as a microfluidic heat sink (figure 10(g)). The performance of such a microfluidic heat sink can be effectively enhanced by a 3D fluid–solid multi-objective and multi-parameter genetic algorithm optimization method. Recently, Zeng and Lee [248] fabricated a liquid-cooled microfluidic heat sink being optimized by using a 3D CFD simulation to achieve a reliable and energy-efficient cooling process (figure 10(h)). Besides, Wang *et al* [249] proposed a solar-powered cooling coating that exhibits remarkable cooling capabilities utilizing atmospheric water.

4.2. Passive mass transfer

The liquid–gas and liquid–liquid two-phase transfer as well as the reaction processes in functional microfluidic devices are also well developed in the past decades. Owing to their excellent hydrodynamic and mass transfer performance, microfluidic systems consisting of programmed microchannels are widely applied, such as droplet transportation, liquid/gas separation, and two-phase reaction. As shown in figure 11(a), Mertaniemi *et al* [105] demonstrated a microfluidic system for transporting droplets based on superhydrophobic technology. Droplets are transported at a high speed in tracks made of hydrophobic microchannels with low friction, enabling the programming of complex trajectories for droplets without any external energy input. In addition, inspired by the beak of shorebirds, Li *et al* [62] proposed a mimetic surface with narrow microchannels realizing directional liquid transportation, demonstrating that unidirectional and bidirectional transport of droplets can be facilely controlled with the change in surface wettability (figure 11(b)). Wang *et al* [153] proposed a bionic functional membrane which can be penetrated by a water droplet within 20 ms from hydrophilic surface to superhydrophilic surface, but the droplets will be blocked in the opposite direction. Significantly, the time it takes for a water droplet to penetrate through the bionic functional surface is much shorter than the time it freezes, even at temperatures as low as −90 °C (figure 11(c)).

Yin *et al* [255] proposed a type of functional microfluidic device to achieve the gas–liquid transfer during CO_2 absorption by embedding baffles in the microchannel. The flow falls into a broken Taylor regime with the increase of the gas flow rate, leading to an ultra-high fluid disturbance and bubbles breakup. Moreover, Xie *et al* [155] proposed a 3D printed bionic cell (figure 11(d)) with superhydrophilic outside surfaces, enabling ultrafast unidirectional water transportation underwater. Chen *et al* [250] also proposed a microfluidic system with 3D splitting structures (figure 11(e)). Owing to the 3D symmetrical microchannels, the microfluidic system can easily split both single and double emulsions into multiple portions. Moreover, Xie *et al* [152] proposed water engine boats with peristome-mimetic structures directionally driven by droplets (figure 11(f)). Such a water fuel boat equipped with five water engines passing through a meter-scale labyrinth as short as 217 s.

The manipulation of droplets using functional microfluidic devices is also attracting more and more attention. Inspired by the heterogeneous wettability of the back of the dessert beetle, directional-dependent architecture of the butterfly wing, and ultraslippery configuration of the *N. alata*, Yang *et al* [251] reported a multi-bioinspired SLIPS-patterned superamphiphobic surface control droplet sliding resistance with precise pattern arrangement, enabling handling of multiple droplets and precise droplet friction control (figure 11(g)). Caggioni *et al* [256] presented the control of droplet shapes through a single microfluidic device only based on the changes in operating conditions. Xie *et al* [69] proposed 3D printed bionic Janus porous matrices which achieve the successful implementation of programmable liquid flow in a desired direction within them working as a precisely printed liquid displayer (figure 11(h)). Zhang *et al* [252] proposed a self-supported monolayered porous polymembrane with special micropores and superhydrophilic–hydrophilic wettability on opposite surfaces (figure 11(i)), achieving the unidirectional transport of droplets. Also, the anti-gravity unidirectional ascent of such a porous membrane in a wide range of pH values can be utilized as a 'liquid diode' for moisture wicking. Moreover, Hu *et al* [253] designed a pneumatic programmable superrepellent surface to tailor conventional wetting materials (such as PDMS) with embedded flexible chambers connected to a microfluidic system (figure 11(j)). Yang *et al* [251] proposed a bionic surface diode with amazing performance of directional droplet sliding and precise control of droplet friction. Zhan *et al* [254] developed a bionic surface with inclined micro-mushrooms for programmable droplet bouncing, offering applications in water transportation, self-cleaning, anti-gravity bouncing, and clean energy generation (figure 11(k)).

4.3. Clean water production

The excellent mass transportation capability enables functional microfluidic devices utilization in the field of solar water evaporation [32]. For such an application, functional microfluidic devices not only transport water but also act as heat insulators after the photothermal conversion with nanostructures [169, 257–262]. Generally speaking, clean water production can be achieved by water absorption from the air and solar vapor generation. Due to the extremely strong water absorption capability of some porous media made of organic materials, the structures can effectively absorb water from the air. As shown in figure 12(a), Fan *et al* [263] developed a 3D MXene-based solar absorber with metal–organic framework-derived carbon nanoplates, achieving efficient solar-driven desalination with high vapor conversion efficiency and stable performance over time. The solar-vapor conversion efficiency of the device can reach around 93.4% and maintain over 91% for 100 h to produce clean vapor for stable

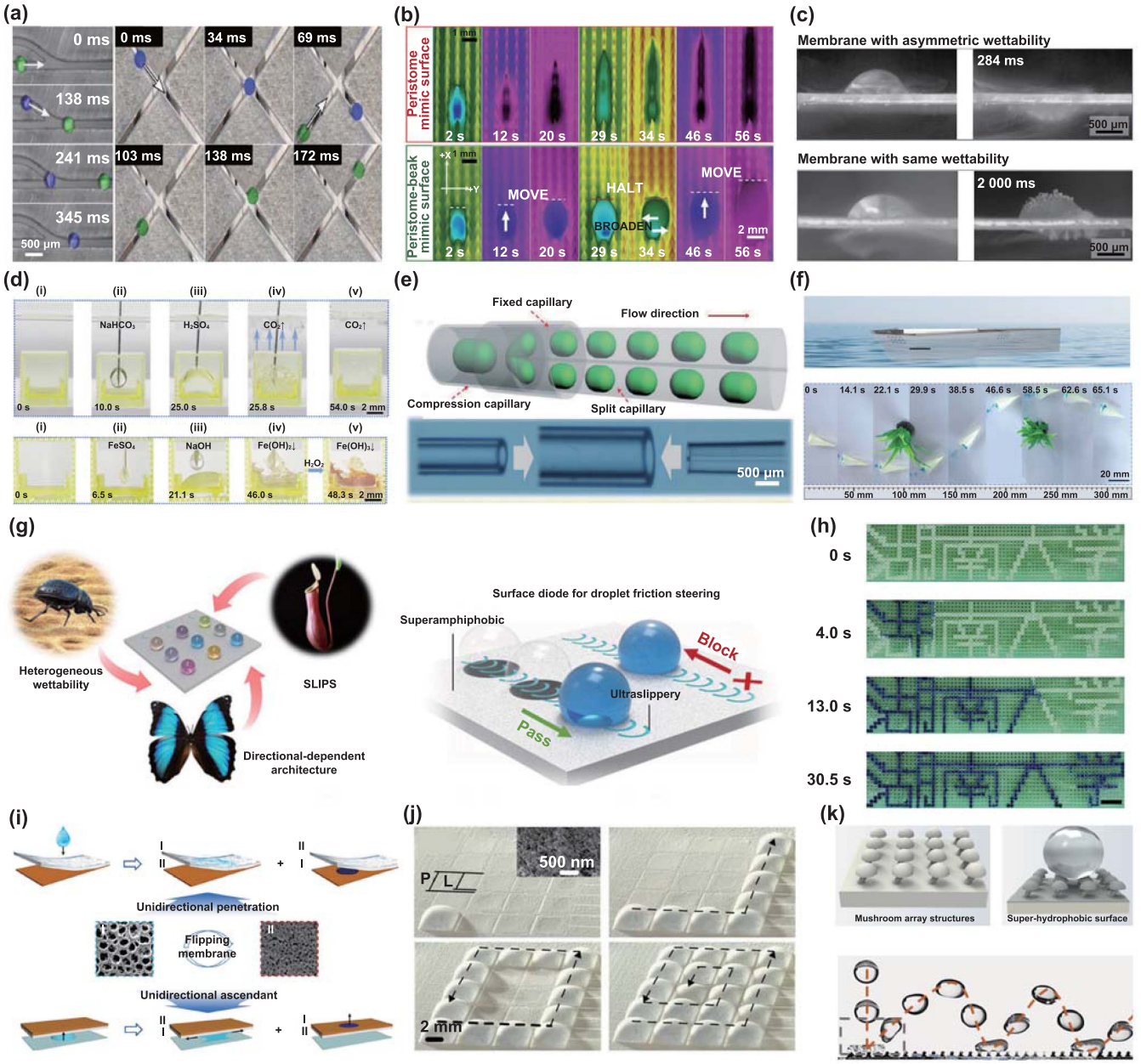

Figure 11. Functional microfluidic devices for passive mass transfer. (a) Low-friction transport of water droplets with superhydrophobic track [105]. [105] John Wiley & Sons. [Copyright © 2011 WILEY-VCH Verlag GmbH & Co. KGaA, Weinheim]. (b) Smart liquid transport with biomimetic surface enabled by temperature fluctuation [62]. [62] John Wiley & Sons. [© 2018 WILEY-VCH Verlag GmbH & Co. KGaA, Weinheim]. (c) A water droplet can penetrate a bionic membrane before being frozen at temperatures as low as −90 °C [153]. Reproduced with permission from [153]. © The Author(s) 2023. Published by Oxford University Press on behalf of National Academy of Sciences. (d) Liquids unidirectional penetration underwater [155]. Reprinted with permission from [155]. Copyright (2022) American Chemical Society. (e) 3D splitting of droplets by the glass functional microfluidic devices [250]. Reproduced from [250] with permission from the Royal Society of Chemistry. (f) Self-driven water boats enabled by Janus membranes [152]. Reprinted from [152], © 2023 Elsevier Ltd. All rights reserved. (g) Multi-bioinspired slippery lubricant-infused porous surface (SLIPS) [251]. Reproduced from [251]. CC BY 4.0. (h) A precisely printed liquid displayer [69]. [69] John Wiley & Sons. [© 2023 Wiley-VCH GmbH]. (i) Unidirectional penetration of liquid enabled by a flexible monolayered porous membrane with superhydrophilic–hydrophilic surfaces [252]. Reprinted with permission from [252]. Copyright (2020) American Chemical Society. (j) A pneumatic programmable superrepellent surface [253]. Reproduced from [253]. CC BY 4.0. (k) A bioinspired functional surface with inclined micromushrooms for programmable and patterned droplet bouncing [254]. [254] John Wiley & Sons. © 2023 Wiley-VCH GmbH.

and continuous water desalination. Besides, inspired by the leaf vein, Lin *et al* [264] proposed four-level wedge tracks for directional water collection (figure 12(b)). Superhydrophilic $Cu(OH)_2$ nanowires are utilized to provide abundant microfluidic paths for promoting droplet absorption and forming water film tracks.

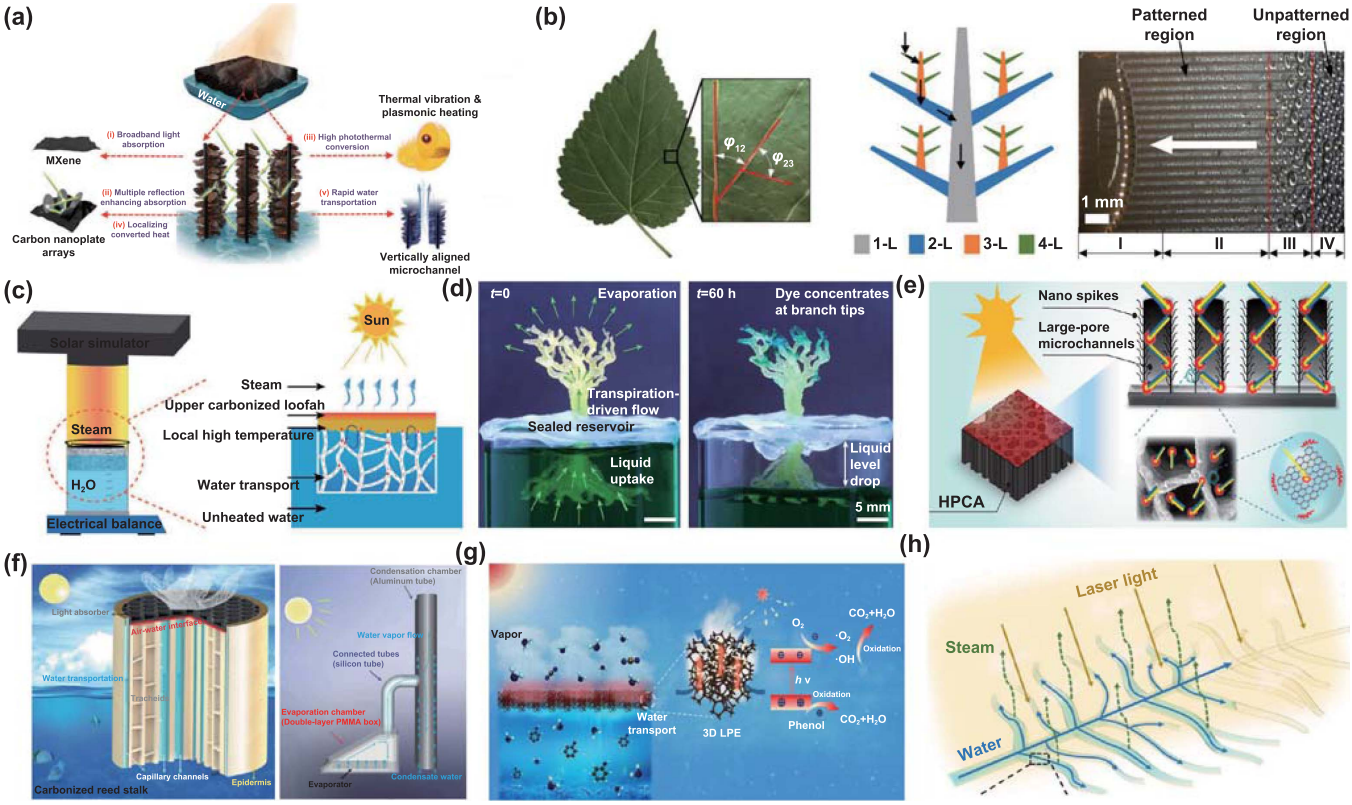

Figure 12. Functional microfluidic devices used in freshwater production. (a) Water absorption from air [263]. [263] John Wiley & Sons. [© 2020 Wiley-VCH GmbH]. (b) Directional water collection with hierarchical wedge tracks [264]. Reprinted with permission from [264]. Copyright (2018) American Chemical Society. (c) Solar thermal desalination by loofah sponge with internal microchannels as water pumps [265]. Reproduced from [265] with permission from the Royal Society of Chemistry. (d) Tree-like functional microfluidic devices for solar water evaporation [266]. Reproduced from [266], with permission from Springer Nature. (e) Bioinspired hierarchical evaporator for solar desalination [267]. Reproduced from [267]. CC BY 4.0. (f) Freshwater collection with a solar evaporator and a passive condenser [268]. Reproduced from [268] with permission from the Royal Society of Chemistry. (g) Light-permeable solar evaporator with 3D functional microfluidic devices for water purification [269]. Reprinted with permission from [269]. Copyright (2022) American Chemical Society. (h) 3D opening functional microfluidic devices for mimicked transpiration [156]. Reprinted with permission from [156]. Copyright (2022) American Chemical Society.

As shown in figure 12(c), a multitude of microchannels are arranged in coarse fibers for rapid vapor transportation during the solar evaporation process [265]. Dudukovic *et al* [266] proposed a microfluidic device based on 3D unit cell structures (figure 12(d)), which achieves deterministic control of multiphase flow as well as reaction processes with a tree-like structure consisting of numerous tetrahedral cells. Inspired by the architecture of leaves in pristine plants, Zhang *et al* [267] presented a bionic photothermal aerogel with numerous microchannels serving as stems (figure 12(e)). Cheng *et al* [268] demonstrated a solar water evaporator with hierarchical carbonized microchannels (figure 12(f)), enabling high water transportation performance and ultralow thermal conductivity. Furthermore, Ma *et al* [269] proposed a 3D volatile organic compound-based solar water evaporator (figure 12(g)). The reactive interface of such a solar evaporator is increased by tens of times compared with a 2D membrane, resulting in a high solar water evaporation efficiency. Inspired by the keratinized membrane at the tip of the hummingbird's tongue, Wang *et al* [156] provided a new strategy for opening functional microfluidic devices working for solar vapor generation (figure 12(h)), which keeps the liquid inside but squeezes out the gas with unique printed openings.

4.4. Microfluidic chips for chemical reactions

Functional microfluidic devices have also been utilized as chemical reaction vessels due to the great mass transfer capability of the microchannels with unique structures and chemical coatings. Guo *et al* [33] proposed a novel 3D serpentine microfluidic reactor (figure 13(a)), which achieves efficient mixing of three different kinds of liquids. Besides, inspired by porous structures by rocks, Ge *et al* [270] proposed a special microfluidic chip with a series of converging-diverging geometries (figure 13(b)), whose mass transfer coefficient is approximately four times to traditional microchannel by increasing the interfacial area. As presented in figure 13(c), Xie *et al* [155] proposed a 3D-printed microfluidic reactor based on unidirectional cellular fluidics, which achieves anaerobic chemical reactions underwater, enabling potential applications in chemical reactions underwater. Moreover, Wang *et al* [156] also reported a bionic open microfluidic device with openings

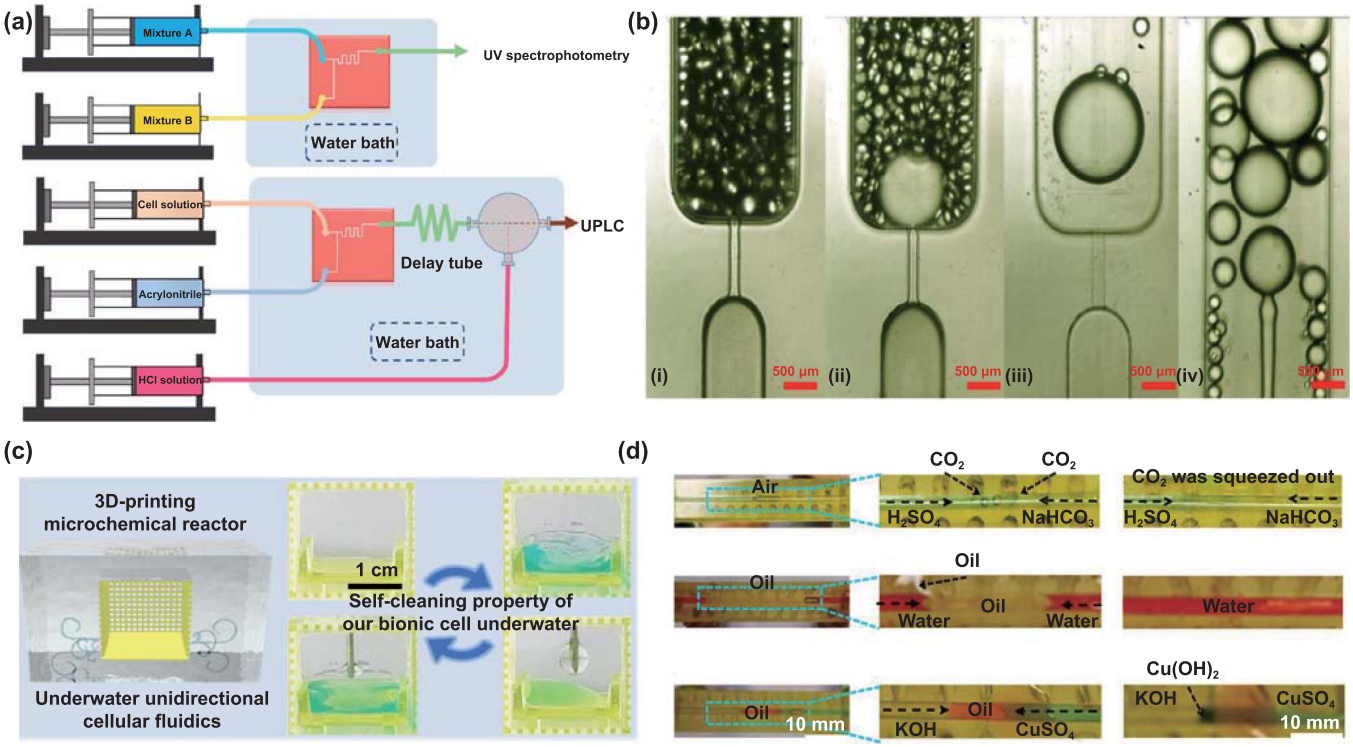

Figure 13. Functional microfluidic devices for chemical reactions. (a) A 3D serpentine microfluidic device with periodic vortex-inducing structure for mixing [33]. Reprinted with permission from [33]. Copyright (2019) American Chemical Society. (b) Solvent extraction enhancement with a series of converging-diverging microfluidic devices [270]. Reprinted from [270], © 2022 Elsevier Ltd. All rights reserved. (c) Complex chemical reactions underwater [155]. Reprinted with permission from [155]. Copyright (2022) American Chemical Society. (d) 3D open microfluidic devices for precise control of chemical reactions [156]. Reprinted with permission from [156]. Copyright (2022) American Chemical Society.

never affected its fluidic performance but discharged gas from the microchannel via the openings (figure 13(d)), solving the severe problem of gaslock in functional microfluidic devices, which can be utilized for precisely controlled chemical reactions, oil–water separation, and controllable drug delivery.

4.5. Microfluidic chip for sensors

With the rapid development of analytical chemistry and MEMS technology, microfluidic chips with complex microchannels are boosting [30]. Owing to the controllable liquid flow inside the microchannels, microfluidic chips achieve fast detection and separation of fluid with low cost. They can also be used to test multiple samples simultaneously, showing considerable application potentials as real-time sensors and chemical detection. As presented in figure 14(a), Zhu *et al* [271] proposed a self-priming fractal-branching microfluidic chip for digital polymerase chain reaction. The fractal tree-like microchannel network structures are inspired by mammalian circulatory and respiratory systems, which achieves sequential reagent loading and isolation for point-of-care detection. In addition, Olanrewaju *et al* [272] developed an advanced capillary microfluidic device that can achieve the autonomous delivery of eight liquids (figure 14(b)). The liquid moves in a pre-programmed drainage order with different hydrostatic pressures to ensure effective real-time detection.

Farmehini *et al* [273] presented a novel circuit implementation for on-chip real-time measurement of resonance frequency and feedback control based on integrated functional microfluidic devices (figure 14(c)). A piezoelectric transducer generates acoustic waves to selectively trap and position target particles in microchannels. Hu *et al* [274] reported a fully integrated and self-contained microfluidic sensor for the automated and quantitative detection of biological hormones (figure 14(d)). The microfluidic device can simultaneously detect 16 samples with a high speed. Ghosh and Ahn [29] reported a microfluidic system using microchannels to form spiral reaction chambers for detecting specific proteins (figure 14(e)). Moreover, Song *et al* [275] proposed a label-free detection method for droplets using microfluidic chips (figure 14(f)). The microscopic device visualizes droplets full-field with high spatiotemporal resolution, which can be used for the observation of the dynamic formation of droplets.

4.6. Biomedical field

Functional microfluidic devices also play a crucial role in biomedical fields, such as regenerative medicine and cell/tissue engineering, which can be employed for cell behavior investigation, drug delivery, tissue regeneration, etc [31]. Compared with other traditional medical testing methods, the use of

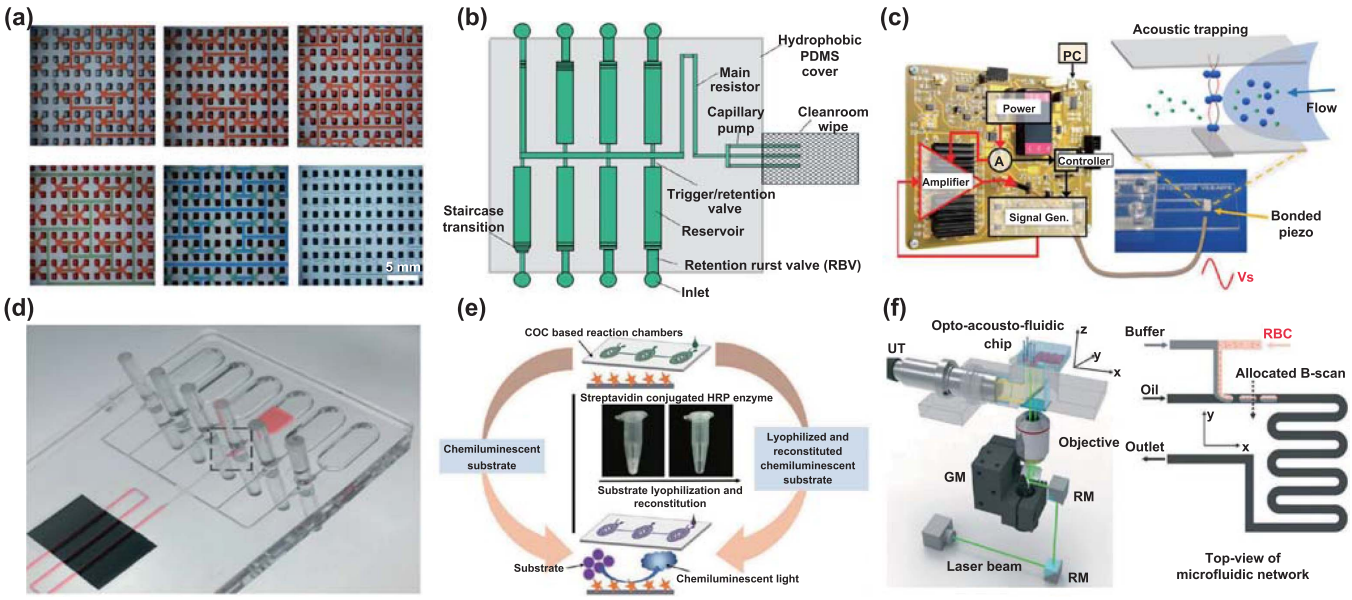

Figure 14. Microfluidic detectors. (a) Large-scale microfluidic net chips with self-priming fractal branching [271]. Reproduced from [271] with permission from the Royal Society of Chemistry. (b) Schematic of microfluidic capillary circuits [272]. Reproduced from [272] with permission from the Royal Society of Chemistry. (c) Microfluidic chips for real-time detection in acoustic trapping systems [273]. Reprinted with permission from [273]. Copyright (2021) American Chemical Society. (d) Quantitative detection of biomarkers enabled by microfluidic chemiluminescence immunoassay [274]. Reproduced from [274] with permission from the Royal Society of Chemistry. (e) Highly sensitive point-of-care diagnostic system with microchannel-based lateral flow assay [29]. Reproduced from [29] with permission from the Royal Society of Chemistry. (f) 3D label-free detection of droplets in microchannels [275]. Reproduced from [275] with permission from the Royal Society of Chemistry.

microfluidic devices can work fast and efficient. For example, Pinho *et al* [276] proposed a novel microfluidic device for the partial extraction of red blood cells in 2013 (figure 15(a)), which achieves red blood cell separation and deformability assessment in a single step, demonstrating a potential diagnostic technique for separating healthy and diseased cells. In addition, Rodrigues *et al* [277] presented a type of microfluidic devices to separate a certain amount of red blood cells without any clogging or jamming (figure 15(b)). Blood cells from initial blood samples can be continuously and simultaneously separated using both cross-flow microfilters and hyperbolic microchannels.

Mane *et al* [278] proposed a T-shaped sealed microchannel to purify motile sperm cells (figure 15(c)). The motile sperm is separated progressively from the fluid flow at the zone near the 'T' junction. Jiang *et al* [279] presented a chitosan scaffold with controllable geometric microchannels using the freeze–drying method (figure 15(d)), demonstrating that functional microfluidic devices can promote cell infiltration and distribution as well as tissue ingrowth. Vu-dinh *et al* [280] proposed a novel microfluidic device specifically for isolating human lung carcinoma in microchannels (figure 15(e)). By exploiting magnetic nanoparticles, the target A549 cells immobilized by magnetic beads can be manipulated by an external magnetic field and trapped in cavities, demonstrating excellent cell separation performance. Tee *et al* [281] adopted a dynamic microcarrier culture platform for chondrocyte expansion (figure 15(f)). Microcarriers with microchannels promote homogenous culture environment, and facilitate oxygen and nutrient transfer, promising a stratified zonal repair of articular cartilage.

4.7. Capillaric circuits

Programmable capillary circuits for the self-powered delivery of liquids are attracting more and more attention in recent years. Based on the capillary force inside functional microfluidic devices, capillaric circuits are widely utilized for the detection, analysis, and viscosity measurement of different fluids. In 2017, Oh *et al* [35] presented a novel 3D-printed microfluidic circuit to analyze the viscosity of the blood. A smart pipette generates controlled shear rate conditions to operate the 3D-printed microfluidic circuit for whole blood analysis (figure 16(a)). Subsequently, Oh and Choi [282] measured the calibration-free viscosity of both Newtonian and non-Newtonian fluids (figure 16(b)). In addition, Yafia *et al* [283] presents a microfluidic chain reaction (MCR) system that allows for the automated control of sequential fluids release for various applications. The MCR system uses capillary domino valves to encode and control the release of fluids from reservoirs in a predetermined order (figure 16(c)). Safavieh and Juncker [284] presents the concept of 'capillarics', which are pre-programmed, self-powered microfluidic circuits built from capillary elements. The authors introduce two novel capillary elements, retention burst valves and low aspect ratio trigger valves, and combine them with other components

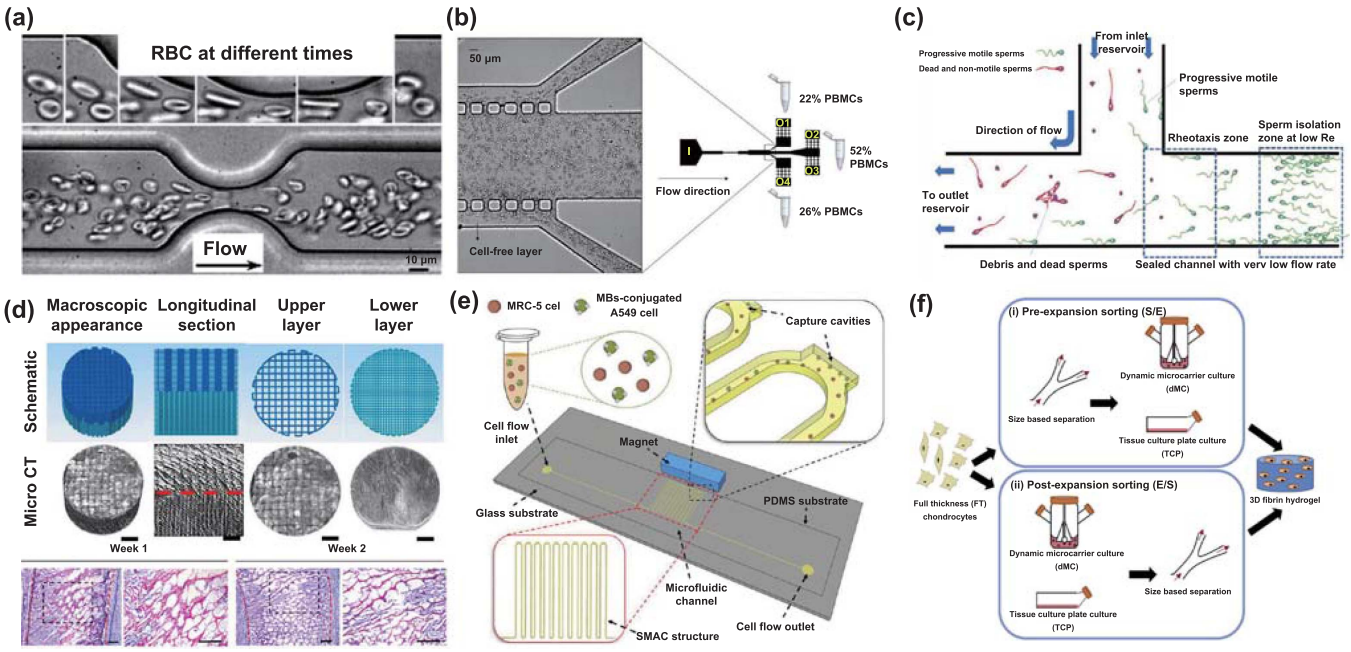

Figure 15. Microfluidic devices used in the biomedical field. (a) Microfluidic devices for deformability assessment and cell separation [276]. Reproduced from [276], with permission from Springer Nature. (b) Red blood cell deformability assessment in continuous flow with microfluidic devices [277]. Reproduced from [277], with permission from Springer Nature. (c) T-shaped sealed microchannels for the separation of motile human sperms [278]. Reproduced from [278], with permission from Springer Nature. (d) Chitosan scaffolds construction with microchannels for tissue engineering [279]. Reprinted from [279], © 2021 Elsevier B.V. All rights reserved. (e) Lung adenocarcinoma cells selection by cavity-added serpentine microchannels [280]. Reproduced from [280], with permission from Springer Nature. (f) Inertial spiral microchannels for clinical applications [281]. Reprinted from [281], © 2019 Elsevier Ltd. All rights reserved.

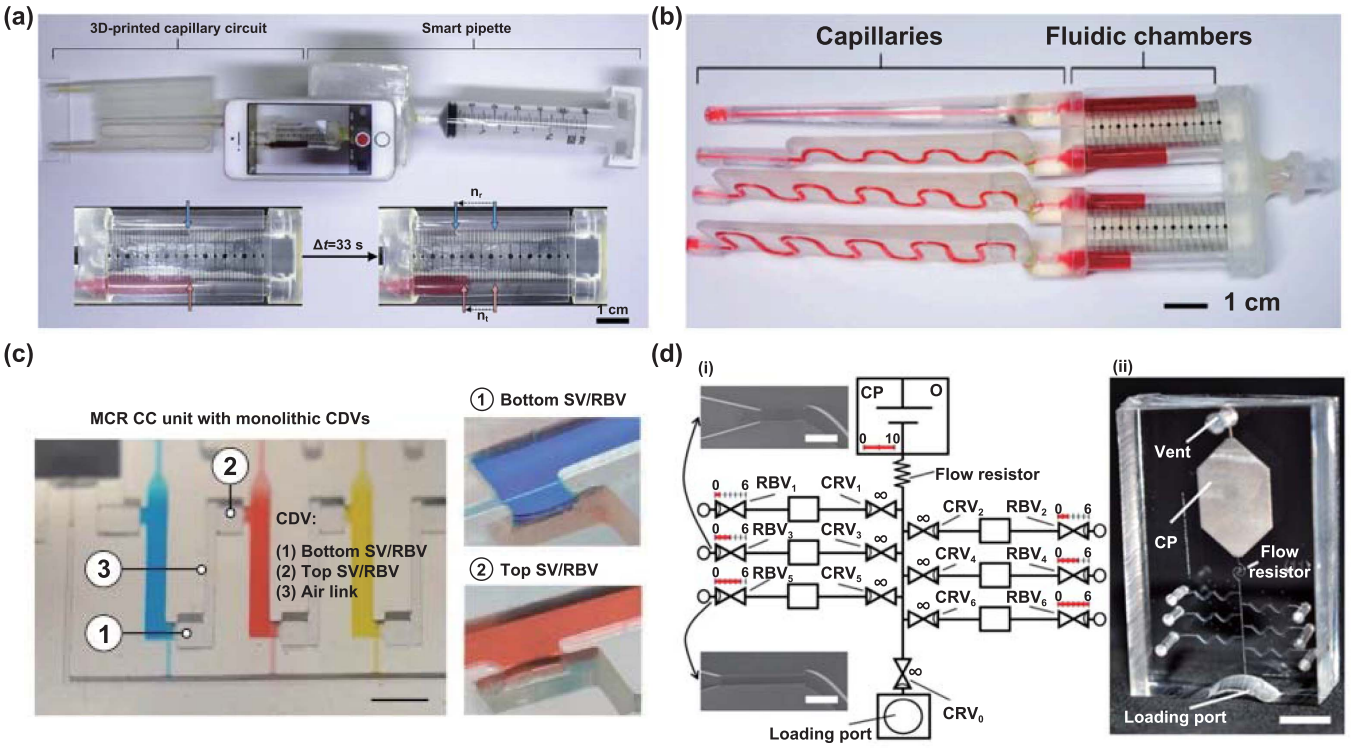

Figure 16. Capillaric circuits. The 3D-printed microfluidic circuits to (a) analyze the blood viscosity [35], Reprinted from [35], © 2017 Elsevier B.V. All rights reserved. As well as (b) measure the calibration-free viscosity of both Newtonian and non-Newtonian fluids [282]. Reproduced from [282]. CC BY 4.0. (c) A microfluidic chain reaction system with a microfluidic capillaric circuit [283]. Reproduced from [283], with permission from Springer Nature. (d) The pre-programmed, self-powered microfluidic circuits which are built from capillary elements [284]. Reproduced from [284] with permission from the Royal Society of Chemistry.

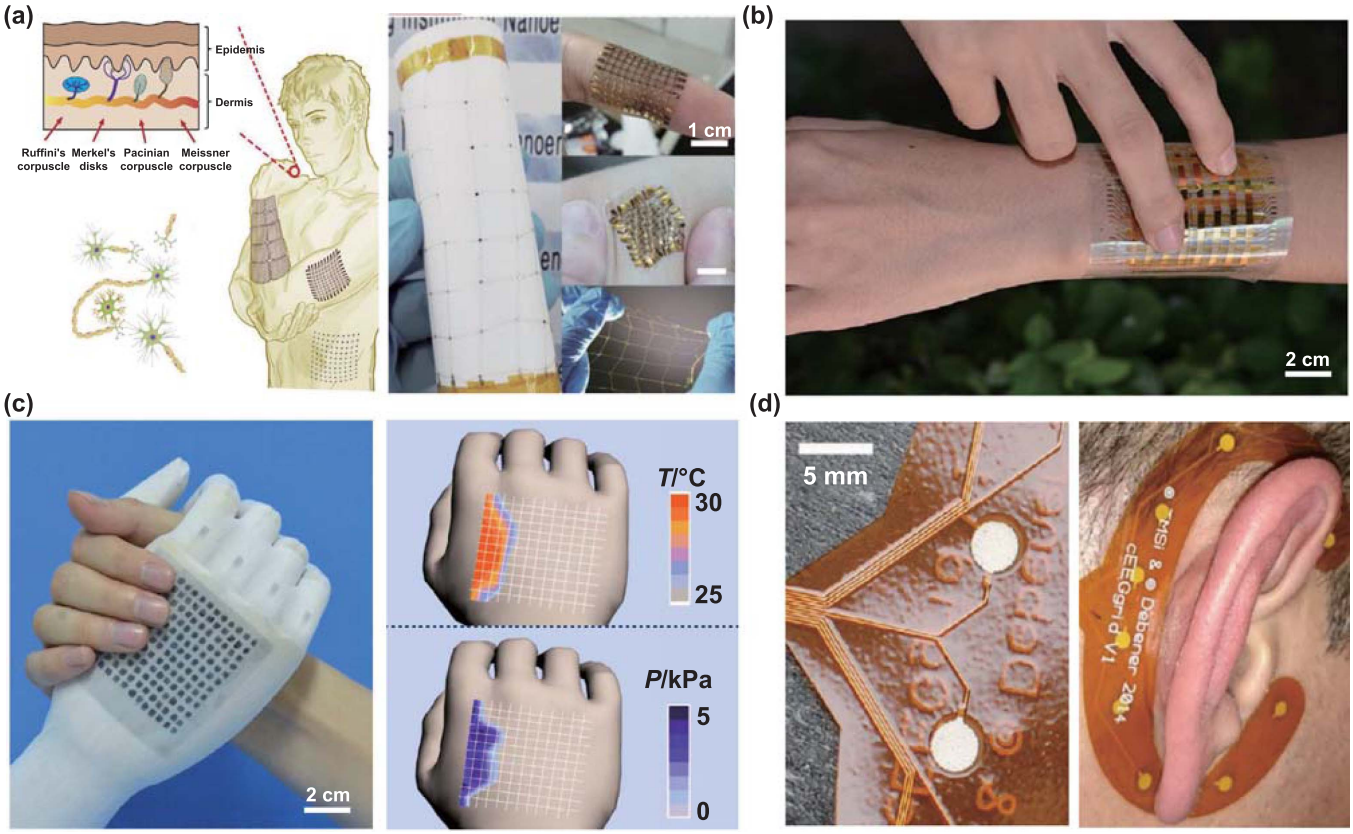

Figure 17. Microfluidic flexible and wearable electronic devices. (a) E-skin sensing with a highly stretchable and conformable microfluidic matrix network inspired by skin [36]. Reproduced from [36]. CC BY 4.0. (b) Ultra-sensitive pressure detection with flexible organic thin-film transistors [285]. Reproduced from [285]. CC BY 4.0. (c) Self-powered flexible dual-parameter sensor for stimuli detection of temperature and pressure [286]. Reproduced from [286]. CC BY 4.0. (d) Electroencephalogram (EEG) signal caption with flexible printed microfluidic electrodes [287]. Reproduced from [287]. CC BY 4.0.

to build a capillary circuit that can autonomously deliver a sequence of multiple chemicals (figure 16(d)).

4.8. Flexible and wearable electronic devices

Microfluidic flexible and wearable electronic devices are also becoming increasingly popular. Microfluidic 'electronic skin' can measure various body parameters, such as heartbeat, blood pressure, concentration of ions, and body temperature. For example, Hua *et al* [36] achieved e-skin sensing of humidity, temperature, magnetic field, in-plane strain, light, proximity, and pressure, with a highly stretchable and conformable matrix microfluidic network inspired by skin (figure 17(a)). Based on such a microfluidic wearable device, various categories of sensing can be achieved with different types of sensor units.

Zang *et al* [285] proposed flexible organic thin-film transistors that enable ultrasensitive pressure detection. As shown in figure 17(b), the electronic devices achieve ultrahigh sensitivity (192 kPa), short response time (less than 10 ms) and low power consumption (less than 100 nW) for real-time sensing of acoustic vibrations and radial artery pulse. Similarly, Zhang *et al* [286] reported a type of flexible sensor for stimuli dual-parameter (temperature and pressure) detection based on microstructures made of organic thermoelectric materials (figure 17(c)). The resolution of temperature detection is less than 0.1 K and the sensitivity for high-pressure-sensing is up to 28.9 kPa for such a flexible sensor. In addition, Debener *et al* [287] proposed microfluidic flexible screen-printed electrodes. As presented in figure 17(d), comfortable and extremely lightweight electrode arrays manufactured with low-cost printed flexible screen technology can detect electroencephalogram (EEG) signals.

4.9. Microrobotics

Advances in soft materials are prompting the development of flexible sensors and actuators for soft robots. For example, Barbot *et al* [37] developed a mobile microfluidic microrobot with 3D motions (figure 18(a)) based on selective self-integration of 3D helical micro-swimmers. In 2021, Ahmed *et al* [288] described a mechanism that used externally triggered acoustic and magnetic fields to transport swarms of microparticles along the boundaries of a microchannel against imposed flow (figure 18(b)). Additionally, Milana *et al* [289] proposed an artificial cilium that imitates the motion of biological cilia with two actuators for independent control, allowing for different asymmetrical motions (figure 18(c)). Based on electrohydrodynamics, Cacucciolo *et al* [40] proposed a type of soft bidirectional pump with charge injection (figure 18(d)). A self-contained fluidic muscle with such an embedded pump

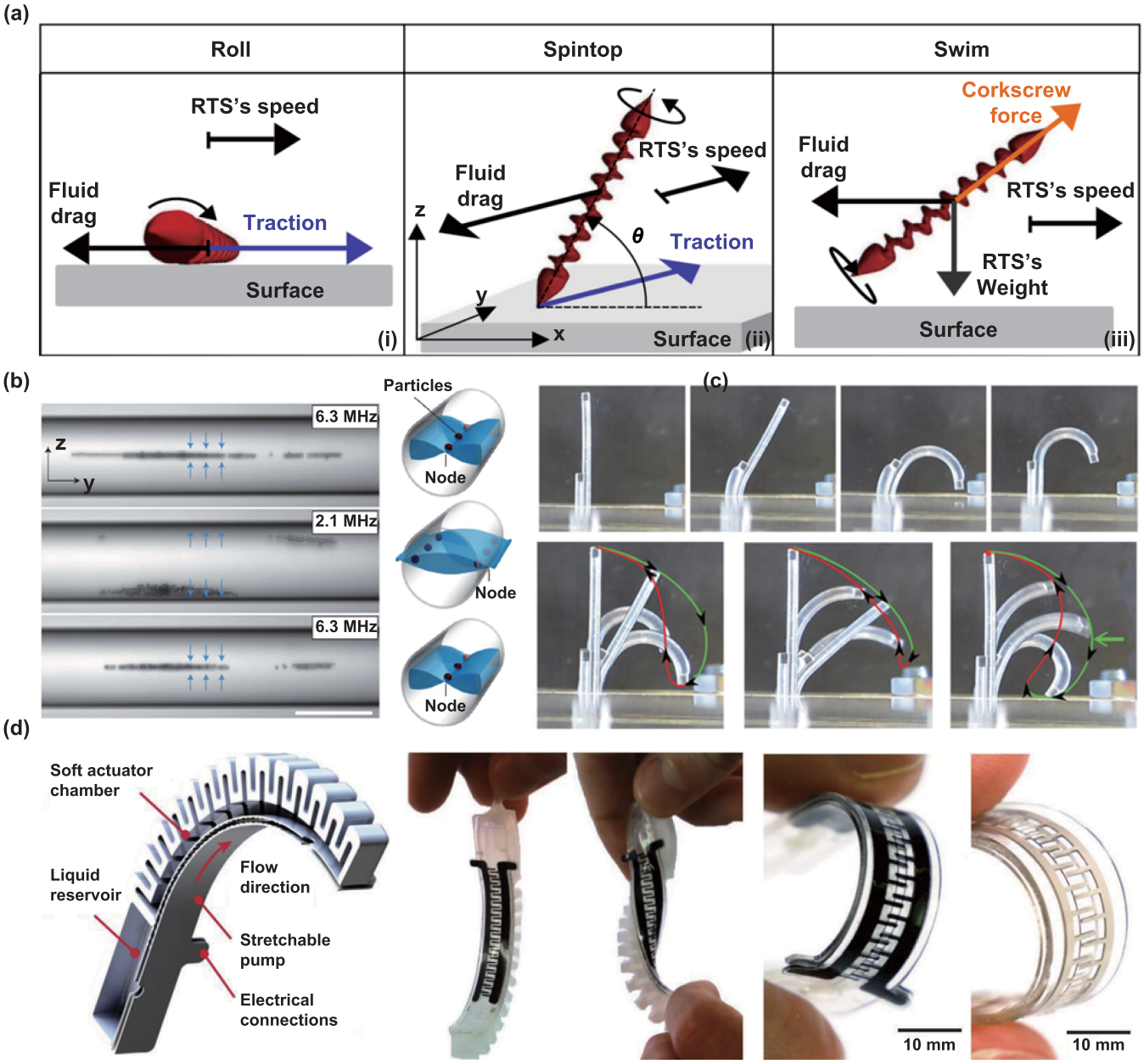

Figure 18. Microfluidic microrobotics. (a) On-chip microfluidic multimodal swimmer for 3D navigation [37]. Reproduced from [37]. CC BY 4.0. (b) Bioinspired acousto-magnetic microswarm robots [288]. Reproduced from [288], with permission from Springer Nature. (c) An artificial cilium mimics the spatial asymmetry of biological cilia's in-plane beating motion [289]. [289] John Wiley & Sons. [© 2019 WILEY-VCH Verlag GmbH & Co. KGaA, Weinheim]. (d) Stretchable pumps for soft machines [40]. Reproduced from [40], with permission from Springer Nature.

can be potentially applied as wearable devices, thermally activated clothing, microfluidic sensors, and autonomous soft robots.

4.10. Fuel cell

Fuel cell is a revolutionary alternative to traditional fuels [290]. Microfluidic devices can increase the reaction area, improve the mass transfer efficiency, reduce the mass transfer resistance, and increase the stability and safety of fuel cells [291]. Braff *et al* [292] reported a microfluidic membrane-free hydrogen bromide laminar flow battery as a potential high power density solution (figure 19(a)). The membraneless design achieved a power density of 0.795 W·cm^{-2} at room temperature and atmospheric pressure with a round-trip voltage efficiency of 25% at 92% of peak power. In addition, proton exchange membranes composed of perfluorinated polyelectrolytes are costly, mechanical strength shortage and dimensional instable. Hence, Yameen *et al* [293] proposed a silicon based multichannels modified with sulfonated polymer brushes, which enabled proton-conducting channels with tailor-made, finely tuned physicochemical characteristics. Regardless of humidity, the highly proton-conducting self-humidifying microchannels generated by copolymer brushes

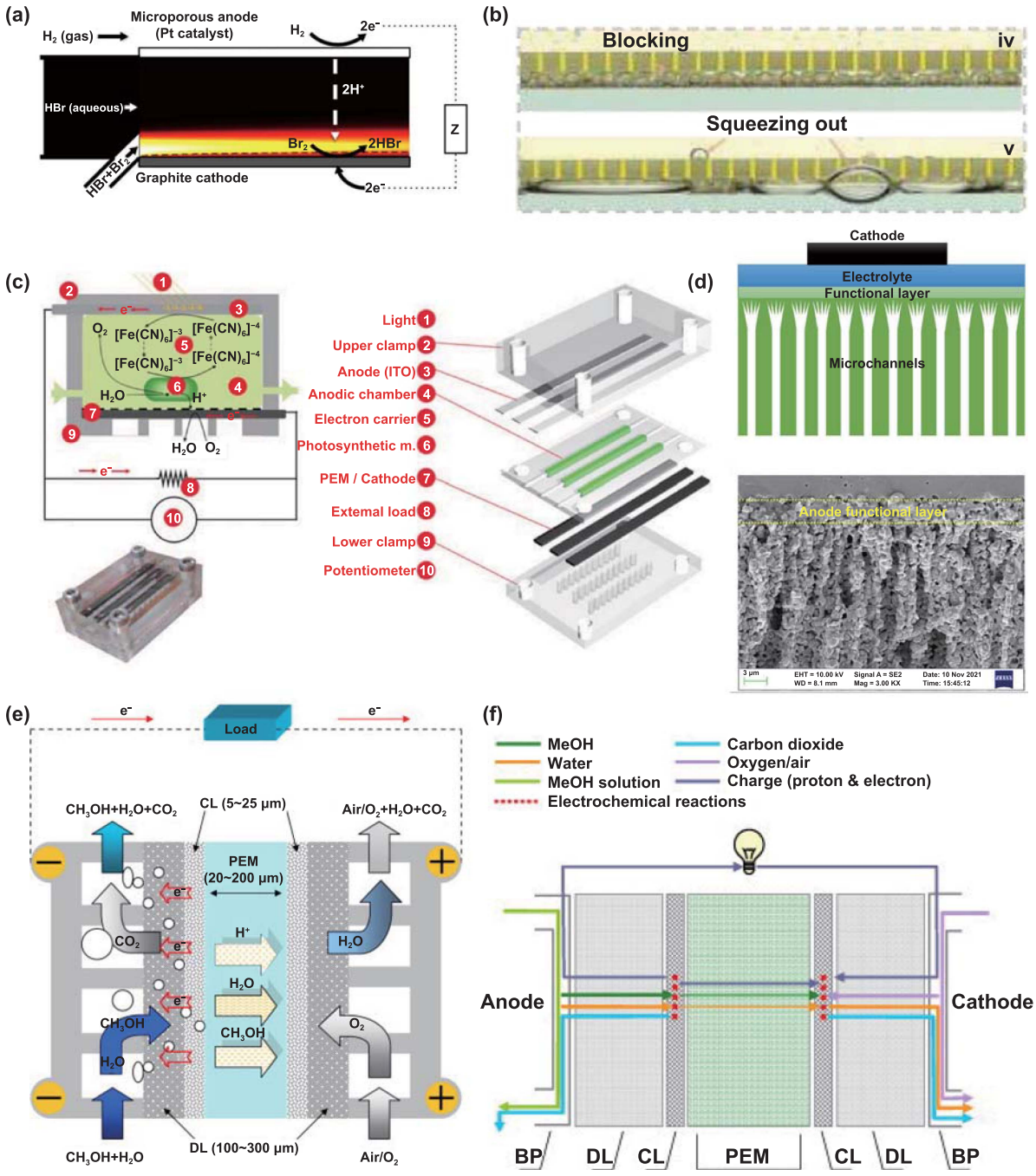

Figure 19. Microfluidic fuel cells. (a) A membrane-less hydrogen bromine laminar flow battery [292]. Reproduced from [292], with permission from Springer Nature. (b) Hydrogen bubbles remove from copper cathode by bionic Janus membranes [294]. Reprinted from [294], © 2023 Elsevier B.V. All rights reserved. (c) A microbial fuel cell -inspired photovoltaic device with multiple microchannels [295]. Reprinted from [295], Copyright (2011), with permission from Elsevier. (d) The SOFC anode integrated with a microfluidic reactor [296]. Reprinted from [296], © 2022 Elsevier Ltd. All rights reserved. (e) Schematic diagram of mass transport phenomena in direct methanol fuel cells with microchannels [297]. Reprinted from [297], Copyright © 2009 Elsevier Ltd. All rights reserved. (f) A portable direct methanol fuel cell [298]. Reprinted from [298], Copyright © 2009 Elsevier B.V. All rights reserved.

on a scaffold display a high conductivity (ca. 10^{-2} S·cm^{-1}), which was much more than that of nafion. Furthermore, Wang *et al* [294] proposed bionic Janus membranes with distinct water-repellent properties on one side, allowing for efficient and rapid transportation of bubbles in one direction underwater. The microholes in the membrane are superhydrophobic, preventing water from entering but allowing for the passage of gas through numerous microchannels. They have successfully utilized these bionic Janus membranes to quickly remove hydrogen bubbles that adhere to the copper cathode during the hydrogen evolution reaction (figure 19(b)).

As shown in figure 19(c), Bombelli *et al* [295] fabricated a microbial fuel cell-inspired photovoltaic device with multiple microchannels, which enabled a straightforward comparison

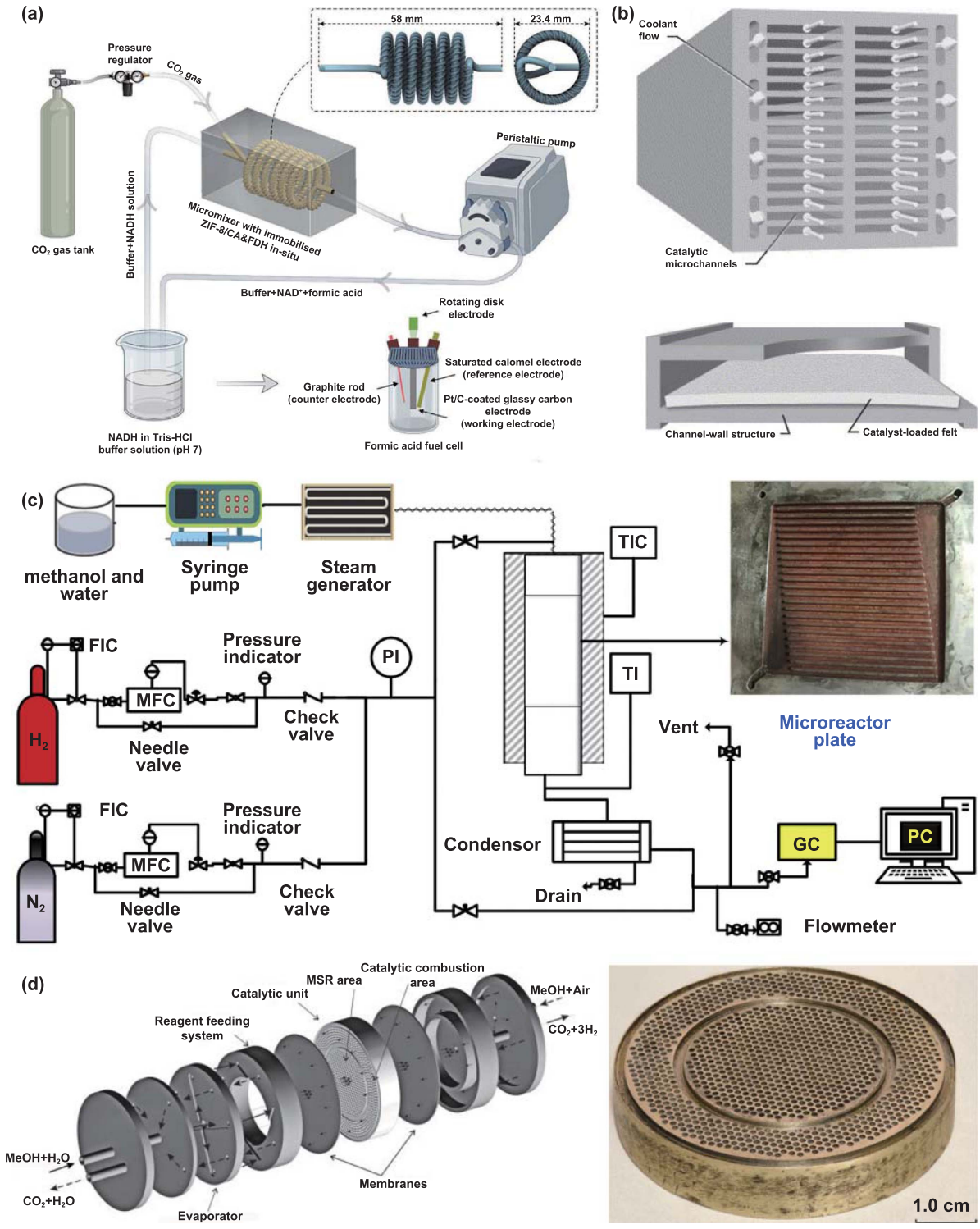

Figure 20. Microfluidic reactors for CO_2 reduction and H_2 production. (a) Schematic diagram of biocatalytic micromixer setups used for the CO_2 reduction [300]. Reprinted from [300], © 2021 Elsevier B.V. All rights reserved. (b) Schematic diagram of a microfluidic reactor, where the reactive gases are directed to flow through the central rectangular microchannels while the outer oval channels are reserved for the flow of oil [301]. Reprinted from [301], Copyright © 2006 Elsevier Ltd. All rights reserved. (c) Schematic of a lab set-up for testing the MSR process [302]. Reprinted from [302], © 2021 Hydrogen Energy Publications LLC. Published by Elsevier Ltd. All rights reserved. (d) A thermally autonomous microfluidic reactor consists of microchannel catalytic units [303]. Reprinted from [303], Copyright © 2015 Elsevier B.V. All rights reserved.

between sub-cellular photosynthetic organelles and entire cells, as well as a quantitative assessment of the factors that affect power generation. Yang *et al* [296] proposed a solid oxide fuel cell (SOFC) anode that consisted of a microfluidic reactor and highly active catalysts (Ni–Y_2O_3–$Ce_{0.5}Zr_{0.5}O_2$) (figure 19(d)). With the help of SOFCs, the conversion rate of

methane was boosted from 23.59% to 43.22% at 750 °C, while the electrochemical output was increased from 905 $mW{\cdot}cm^{-2}$ to 1208 $mW{\cdot}cm^{-2}$. Additionally, there was a significant improvement for the ability to resist coking of the fuel cells. Zhao *et al* [297] designed a direct methanol fuel cell (DMFC) with microchannels (figure 19(e)). It is revealed that bubbles formation and elimination occurred periodically due to transient capillary blockage in small flow microchannels. The reduction in microchannel width led to an increase in the length of gas slugs and the duration of gas slug blockage in the flow channels. Zhao *et al* [298] devised a fuel-delivery system comprising a fuel reservoir (figure 19(f)). Methanol is conveyed from the fuel reservoir through the porous plate and the openings of the current-collector to reach the anode. At the same time, the CO_2 generated at the anode electrode is transported through the same components, but in the opposite direction. The DMFC system enabled a relatively high performance with nearly pure methanol (22.0 M) as the fuel source.

4.11. Microfluidic reactors for CO_2 reduction and H_2 production

Microfluidic devices provide efficient gas-liquid interfaces that facilitate the mixing and transfer of reactants while controlling the temperature and pressure of the reactions [299]. Chai *et al* [300] designed a novel micromixer with 3D helical, threaded microchannels (figure 20(a)) for CO_2 conversion to formic acid via enzymatic cascade reaction. Optimum performance was observed with a liquid flow rate of 1 $ml{\cdot}min^{-1}$. Brooks *et al* [301] proposed a microfluidic Sabatier reactor for the methanation of CO_2 by hydrogen reduction to produce H_2O and CH_4 (figure 20(b)), which offers efficient heat and mass transfer between the reactive-gas flow and the channel walls, resulting in precise temperature control within a compact reactor system for CO_2 reduction.

Similarly, microfluidic devices can also provide highly controlled reaction conditions for H_2 production, including parameters such as temperature, pressure and flow rate for efficient hydrolysis reactions that split water into hydrogen and oxygen while controlling the purity and flow of reaction products [304]. Khani *et al* [302] synthesized a new composite consisting of cerium, yttrium, and ruthenium as a support in the methanol steam reforming (MSR) process for copper metal (figure 20(c)), resulting in exceptional methanol conversion rates and product selectivity. Gribovskiy *et al* [303] manufactured a thermally autonomous microfluidic reactor with a microchannel catalytic unit (MCU) containing a catalyst for hydrogen production in the steam reforming of methanol (figure 20(d)). The high thermal conductivity of the MCU along with the narrow cross-sectional area of its channels facilitates efficient heat and mass transfer, resulting in isothermal conditions.

5. Conclusion and perspective

This paper reviews the functional microfluidic devices mainly from the viewpoints of the driving force, manufacturing methods and various promising applications. First, capillary theory has been built based on the wettability of a surface in the past four centuries. Second, the fabrication of microchannels has been greatly developed in the past half century, including the materials, fabrication methods, post-treatment, and so on. Last and the most significant, various applications based on functional microfluidic devices have been proposed in the past three decades, such as heat sinks, diagnostics, detection, biomedical engineering, production of materials, capillaric circuits, flexible and wearable electronic devices, and microrobotics. All the pieces of evidence have strongly demonstrated that functional microfluidic devices promise new capabilities for the future because much technology needs to be developed to manipulate liquids and gas in various functional devices.

Although significant advances have been achieved in such a promising field, much effort is still needed to address big challenges in functional microfluidic devices ahead. First, a general analytical solution for capillary force theory to various microchannels needs to be obtained because the present ones are only suitable for smooth microchannels, while complex microchannels with inner micro/nanostructures are the future. Second, materials and related fabrication methods for functional microfluidic devices are still in their fancy. For example, there is only few functional microfluidic devices with inner micro/nanostructures proposed in the past, and the large-scale fabrication methods with extremely high precision for complex microfluidic devices are almost impossible except for the newly developed 3D printing techniques. Finally, limited by the shortcomings mentioned above, the applications of functional microfluidic devices are far from meeting expectations. For example, the gaslock inside microchannels severely limits almost all applications related to two phase flow with gas, it is far from satisfactory, though our group at Hunan University is trying to solve such a problem now. Also, functional microfluidic devices should be developed interdisciplinarily in corporations with artificial intelligence, bionic engineering, etc.

Regarding those various promising applications for functional microfluidic devices now and in the future, their applications in the field of carbon neutrality should be emphasized. For example, special pesticides are needed to enhance their utilization efficiency and lower the pollution of the land by enhancing their attachment to the leaves enabled by wettability. In addition, flow cells strongly depend on the microfluidic performance of the microfluidic systems, and special micro-matrices suppress lithium dendrite growth. Furthermore, almost all the electrodes for hydrogen evolution and CO_2 reduction are porous media, no matter carbon paper electrodes, foam nickel, or others, and large-scale functional microfluidic electrodes are one of the promising candidates for those kinds of carbon neutral catalytic electrodes. Most significantly, the exploration of space is attracting more and more attention all over the world, and most of those planned processes related to liquid and gas are supposed to depend on functional microfluidic devices under microgravity conditions. We prospect the rapid development of novel integrated functional microfluidic devices, no matter in theory, materials, manufacturing methods, applications, which are so important

to reshape our understanding of numerous physical and chemical processes, which will benefit our carbon neutral daily life soon.

Data and materials availability

All data needed to evaluate the conclusions in the paper are present in the paper. Additional data related to this paper may be requested from the corresponding authors upon reasonable request.

Funding

This work was supported by the National Natural Science Foundation of China (52006056) and the Key-Area Research and Development Program of Guangdong Province (2020B090923003). The project was also partly supported by Natural Research Institute for Family Planning as well.

Conflict of interest

The authors declare no conflict of interest.

ORCID iD

Zhaolong Wang https://orcid.org/0000-0003-2967-4546

References

[1] Da Vinci L 2012 *The Notebooks of Leonardo da Vinci* (CreateSpace Independent Publishing)
[2] Jurin J 1718 II. An account of some experiments shown before the Royal Society; with an enquiry into the cause of the ascent and suspension of water in capillary tubes *Phil. Trans.* **30** 739–47
[3] Pomeau Y and Villermaux E 2006 Two hundred years of capillarity research *Phys. Today* **59** 39–44
[4] de Laplace P S 1835 *Oeuvres complètes de Laplace* (Gautier-Villars)
[5] Hwang S T 1977 The Gauss equation in capillarity *Z. Phys. Chem.* **105** 225–35
[6] Gibbs J W 1906 *The Scientific Papers of J. Willard Gibbs* (Longmans, Green and Company)
[7] Lomax H, Pulliam T H and Zingg D W 2001 *Fundamentals of Computational Fluid Dynamics* (Springer)
[8] van Gunsteren W F and Berendsen H J C 1990 Computer simulation of molecular dynamics: methodology, applications, and perspectives in chemistry *Angew. Chem., Int. Ed.* **29** 992–1023
[9] Chen S Y and Doolen G D 1998 Lattice Boltzmann method for fluid flows *Annu. Rev. Fluid Mech.* **30** 329–64
[10] LeBeau G J and Lumpkin I I I F E 2001 Application highlights of the DSMC analysis code (DAC) software for simulating rarefied flows *Comput. Methods Appl. Mech. Eng.* **191** 595–609
[11] Terry S C, Jerman J H and Angell J B 1979 A gas chromatographic air analyzer fabricated on a silicon wafer *IEEE Trans. Electron Dev.* **26** 1880–6
[12] Manz A, Graber N and Widmer H M 1990 Miniaturized total chemical analysis systems: a novel concept for chemical sensing *Sens. Actuators* B **1** 244–8
[13] McDonald J C, Duffy D C, Anderson J R, Chiu D T, Wu H K, Schueller O J A and Whitesides G M 2000 Fabrication of microfluidic systems in poly(dimethylsiloxane) *Electrophoresis* **21** 27–40
[14] Martynova L, Locascio L E, Gaitan M, Kramer G W, Christensen R G and MacCrehan W A 1997 Fabrication of plastic microfluid channels by imprinting methods *Anal. Chem.* **69** 4783–9
[15] Zhu W *et al* 2018 Rapid continuous 3D printing of customizable peripheral nerve guidance conduits *Mater. Today* **21** 951–9
[16] Pan D *et al* 2021 Transparent light-driven hydrogel actuator based on photothermal Marangoni effect and buoyancy flow for three-dimensional motion *Adv. Funct. Mater.* **31** 2009386
[17] Zhang H, Sun L Y, Guo J H and Zhao Y J 2023 Hierarchical spinning of Janus textiles with anisotropic wettability for wound healing *Research* **6** 0129
[18] Chen L, Duan G H, Zhang C, Cheng P and Wang Z L 2022 3D printed hydrogel for soft thermo-responsive smart window *Int. J. Extrem. Manuf.* **4** 025302
[19] Kurihara K, Hokari R and Takada N 2021 Capillary effect enhancement in a plastic capillary tube by nanostructured surface *Polymers* **13** 628
[20] Martinez A W, Phillips S T, Butte M J and Whitesides G M 2007 Patterned paper as a platform for inexpensive, low-volume, portable bioassays *Angew. Chem.* **119** 1340–2
[21] Yuan R, Lee J, Su H W, Levy E, Khudiyev T, Voldman J and Fink Y 2018 Microfluidics in structured multimaterial fibers *Proc. Natl Acad. Sci. USA* **115** E10830–8
[22] Ge Q, Li Z Q, Wang Z L, Kowsari K, Zhang W, He X N, Zhou J L and Fang N X 2020 Projection micro stereolithography based 3D printing and its applications *Int. J. Extrem. Manuf.* **2** 022004
[23] Sun Q S, Xue Z X, Chen Y, Xia R D, Wang J M, Xu S, Zhang J and Yue Y N 2022 Modulation of the thermal transport of micro-structured materials from 3D printing *Int. J. Extrem. Manuf.* **4** 015001
[24] Han W, Kong L B and Xu M 2022 Advances in selective laser sintering of polymers *Int. J. Extrem. Manuf.* **4** 042002
[25] Wang Z L, Yin Q, Zhan Z H, Li W H, Xie M Z, Duan H G, Cheng P, Zhang C, Chen Y P and Dong Z C 2023 Bionic microchannels for step lifting transpiration *Int. J. Extrem. Manuf.* **5** 025502
[26] Whitesides G M 2006 The origins and the future of microfluidics *Nature* **442** 368–73
[27] Wu H Y and Cheng P 2003 An experimental study of convective heat transfer in silicon microchannels with different surface conditions *Int. J. Heat Mass Transfer* **46** 2547–56
[28] Kang Z X, Jiang S K, Hong Y and Fan J T 2022 Squid-like soft heat pipe for multiple heat transport *Droplet* **1** 182–91
[29] Ghosh S and Ahn C H 2019 Lyophilization of chemiluminescent substrate reagents for high-sensitive microchannel-based lateral flow assay (MLFA) in point-of-care (POC) diagnostic system *Analyst* **144** 2109–19
[30] Zhang J, Yan S, Sluyter R, Li W H, Alici G and Nguyen N T 2014 Inertial particle separation by differential equilibrium positions in a symmetrical serpentine micro-channel *Sci. Rep.* **4** 4527
[31] Wang M, Cheng B, Yang Y W, Liu H, Huang G Y, Han L C, Li F and Xu F 2019 Microchannel stiffness and confinement jointly induce the mesenchymal-amoeboid transition of cancer cell migration *Nano Lett.* **19** 5949–58

[32] Rony R U and Gladen A 2021 Parametric study and sensitivity analysis of a PV/microchannel direct-expansion CO_2 heat pump *Sol. Energy* **218** 282–95

[33] Guo M Z, Hu X J, Yang F, Jiao S, Wang Y J, Zhao H Y, Luo G S and Yu H M 2019 Mixing performance and application of a three-dimensional serpentine microchannel reactor with a periodic vortex-inducing structure *Ind. Eng. Chem. Res.* **58** 13357–65

[34] Wu D, Ding Y L, Zhang Y X, Pan D, Li J W, Hu Y L, Xu B and Chu J R 2021 3D microfluidic cloth-based analytical devices on a single piece of cloth by one-step laser hydrophilicity modification *Lab Chip* **21** 4805–13

[35] Oh S, Kim B, Lee J K and Choi S 2018 3D-printed capillary circuits for rapid, low-cost, portable analysis of blood viscosity *Sens. Actuators* B **259** 106–13

[36] Hua Q L, Sun J L, Liu H T, Bao R R, Yu R M, Zhai J Y, Pan C F and Wang Z L 2018 Skin-inspired highly stretchable and conformable matrix networks for multifunctional sensing *Nat. Commun.* **9** 244

[37] Barbot A, Decanini D and Hwang G 2016 On-chip microfluidic multimodal swimmer toward 3D navigation *Sci. Rep.* **6** 19041

[38] Zhan Z H, Chen L, Duan H G, Chen Y Q, He M and Wang Z L 2022 3D printed ultra-fast photothermal responsive shape memory hydrogel for microrobots *Int. J. Extrem. Manuf.* **4** 015302

[39] Yang Y Q and Lee C 2022 Making use of water droplets as a sustainable green energy source *Droplet* **1** 7–10

[40] Cacucciolo V, Shintake J, Kuwajima Y, Maeda S, Floreano D and Shea H 2019 Stretchable pumps for soft machines *Nature* **572** 516–9

[41] Yin Q, Guo Q, Wang Z L, Chen Y Q, Duan H G and Cheng P 2021 3D-printed bioinspired Cassie-Baxter wettability for controllable microdroplet manipulation *ACS Appl. Mater. Interfaces* **13** 1979–87

[42] Xu J K, Xiu S, Lian Z X, Yu H D and Cao J J 2022 Bioinspired materials for droplet manipulation: principles, methods and applications *Droplet* **1** 11–37

[43] Gulfam R and Chen Y P 2022 Recent growth of wettability gradient surfaces: a review *Research* **2022** 9873075

[44] Zhao Z P, Li H Z, Liu Q, Li A, Xue L L, Yuan R X, Yu X Y, Li R J, Deng X and Song Y L 2023 Regulating droplet impact symmetry by surface engineering *Droplet* **2** e52

[45] Sun Z N, Zeng X, Deng X, Zhang X S and Zhang Y 2023 Droplet interface in additive manufacturing: from process to application *Droplet* **2** e57

[46] Yu F F, Yang J L, Tao R, Tan Y, Wang J P, Wang D H, Chen L Q, Wang Z K and Deng X 2023 Aerodynamic super-repellent surfaces *Research* **6** 0111

[47] Liang X C, Kumar V, Ahmadi F and Zhu Y Y 2022 Manipulation of droplets and bubbles for thermal applications *Droplet* **1** 80–91

[48] Young T 1805 III. An essay on the cohesion of fluids *Phil. Trans.* **95** 65–87

[49] Chen C, Huang Z C, Zhu S W, Liu B R, Li J W, Hu Y L, Wu D and Chu J R 2021 In situ electric-induced switchable transparency and wettability on laser-ablated bioinspired paraffin-impregnated slippery surfaces *Adv. Sci.* **8** 2100701

[50] Lin F Y H, Li D and Neumann A W 1993 Effect of surface roughness on the dependence of contact angles on drop size *J. Colloid Interface Sci.* **159** 86–95

[51] Wenzel R N 1936 Resistance of solid surfaces to wetting by water *Ind. Eng. Chem.* **28** 988–94

[52] Cassie A B D and Baxter S 1944 Wettability of porous surfaces *Trans. Faraday Soc.* **40** 546–51

[53] Koishi T, Yasuoka K, Fujikawa S, Ebisuzaki T and Zeng X C 2009 Coexistence and transition between Cassie and Wenzel state on pillared hydrophobic surface *Proc. Natl Acad. Sci. USA* **106** 8435–40

[54] Bormashenko E 2015 Progress in understanding wetting transitions on rough surfaces *Adv. Colloid Interface Sci.* **222** 92–103

[55] Leng X, Sun L C, Long Y J and Lu Y 2022 Bioinspired superwetting materials for water manipulation *Droplet* **1** 139–69

[56] Zheng Y P, Xu M, Zhao J C, Zhang B C, Bei S Q and Hao L H 2011 Morphological adaptations to drought and reproductive strategy of the moss *Syntrichia caninervis* in the Gurbantunggut Desert, China *Arid Land Res. Manage.* **25** 116–27

[57] Ju J, Bai H, Zheng Y M, Zhao T Y, Fang R C and Jiang L 2012 A multi-structural and multi-functional integrated fog collection system in cactus *Nat. Commun.* **3** 1247

[58] Parker A R and Lawrence C R 2001 Water capture by a desert beetle *Nature* **414** 33–34

[59] Konrad W, Roth-Nebelsick A, Kessel B, Miranda T, Ebner M, Schott R and Nebelsick J H 2021 The impact of raindrops on *Salvinia molesta* leaves: effects of trichomes and elasticity *J. R. Soc. Interface* **18** 20210676

[60] Liu X J, Li B Y, Gu Z Z and Zhou K 2023 4D printing of butterfly scale–inspired structures for wide-angle directional liquid transport *Small* **19** 2207640

[61] Gao X F and Jiang L 2004 Water-repellent legs of water striders *Nature* **432** 36

[62] Li C X, Yu C L, Hao D Z, Wu L, Dong Z C and Jiang L 2018 Smart liquid transport on dual biomimetic surface via temperature fluctuation control *Adv. Funct. Mater.* **28** 1707490

[63] Tian Y, Zhu P G, Tang X, Zhou C M, Wang J M, Kong T T, Xu M and Wang L Q 2017 Large-scale water collection of bioinspired cavity-microfibers *Nat. Commun.* **8** 1080

[64] Prakash M, Quéré D and Bush J W M 2008 Surface tension transport of prey by feeding shorebirds: the capillary ratchet *Science* **320** 931–4

[65] Peng Y B, Jiao Y L, Li C Z, Zhu S W, Chen C, Hu Y L, Li J W, Cao Y Y and Wu D 2022 Meniscus-induced directional self-transport of submerged bubbles on a slippery oil-infused pillar array with height-gradient *Langmuir* **38** 15001–7

[66] Mason G and Morrow N R 1984 Meniscus curvatures in capillaries of uniform cross-section *J. Chem. Soc. Faraday Trans. 1* **80** 2375–93

[67] Fisher L R, Gamble R A and Middlehurst J 1981 The Kelvin equation and the capillary condensation of water *Nature* **290** 575–6

[68] Washburn E W 1921 The dynamics of capillary flow *Phys. Rev.* **17** 273–83

[69] Xie M Z, Zhan Z H, Zhang C Q, Xu W Q, Zhang C, Chen Y P, Dong Z C and Wang Z L 2023 Programmable microfluidics enabled by 3D printed bionic Janus porous matrices for microfluidic logic chips *Small* **19** 2300047

[70] Elizalde E, Urteaga R, Koropecki R R and Berli C L 2014 Inverse problem of capillary filling *Phys. Rev. Lett.* **112** 134502

[71] Tao R, Fang W, Wu J, Dou B H, Xu W H, Zheng Z Y, Li B, Wang Z K, Feng X Q and Hao C L 2023 Rotating surfaces promote the shedding of droplets *Research* **6** 0023

[72] Dai H Y, Gao C, Sun J H, Li C X, Li N, Wu L, Dong Z C and Jiang L 2019 Controllable high-speed electrostatic manipulation of water droplets on a superhydrophobic surface *Adv. Mater.* **31** 1905449

[73] Li J, Ha N S, Liu T Y, van Dam R M and Kim C J 2019 Ionic-surfactant-mediated electro-dewetting for digital microfluidics *Nature* **572** 507–10

[74] Kwon G, Panchanathan D, Mahmoudi S R, Gondal M A, McKinley G H and Varanasi K K 2017 Visible light guided manipulation of liquid wettability on photoresponsive surfaces *Nat. Commun.* **8** 14968
[75] Zhang Y and Nguyen N T 2017 Magnetic digital microfluidics–a review *Lab Chip* **17** 994–1008
[76] Barani A, Paktinat H, Janmaleki M, Mohammadi A, Mosaddegh P, Fadaei-Tehrani A and Sanati-Nezhad A 2016 Microfluidic integrated acoustic waving for manipulation of cells and molecules *Biosens. Bioelectron.* **85** 714–25
[77] Li H and Olsen M G 2006 MicroPIV measurements of turbulent flow in square microchannels with hydraulic diameters from 200 μm to 640 μm *Int. J. Heat Fluid Flow* **27** 123–34
[78] Moukalled F, Mangani L and Darwish M 2016 The finite volume method *The Finite Volume Method in Computational Fluid Dynamics* ed F Moukalled, L Mangani and M Darwish (Springer)
[79] Alder B J and Wainwright T E 1959 Studies in molecular dynamics. I. General method *J. Chem. Phys.* **31** 459–66
[80] Bird G A 1998 Recent advances and current challenges for DSMC *Comput. Math. Appl.* **35** 1–14
[81] Nagayama G and Cheng P 2004 Effects of interface wettability on microscale flow by molecular dynamics simulation *Int. J. Heat Mass Transfer* **47** 501–13
[82] Felippa C A 2004 *Introduction to Finite Element Methods* (University of Colorado)
[83] Godunov S K and Bohachevsky I 1959 Finite difference method for numerical computation of discontinuous solutions of the equations of fluid dynamics *Mat. Sb.* **47** 271–306
[84] Lindahl E and Edholm O 2000 Mesoscopic undulations and thickness fluctuations in lipid bilayers from molecular dynamics simulations *Biophys. J.* **79** 426–33
[85] Martic G, Gentner F, Seveno D, Coulon D, De Coninck J and Blake T D 2002 A molecular dynamics simulation of capillary imbibition *Langmuir* **18** 7971–6
[86] Koplik J, Banavar J R and Willemsen J F 1988 Molecular dynamics of Poiseuille flow and moving contact lines *Phys. Rev. Lett.* **60** 1282–5
[87] Guo Z L and Shu C 2013 *Lattice Boltzmann Method and Its Applications in Engineering* (World Scientific)
[88] Benzi R, Succi S and Vergassola M 1992 The lattice Boltzmann equation: theory and applications *Phys. Rep.* **222** 145–97
[89] Chen S Y, Martínez D and Mei R W 1996 On boundary conditions in lattice Boltzmann methods *Phys. Fluids* **8** 2527–36
[90] Spaid M A A and Phelan F R Jr 1997 Lattice Boltzmann methods for modeling microscale flow in fibrous porous media *Phys. Fluids* **9** 2468–74
[91] Van der Graaf S, Nisisako T, Schroën C G P H, Van Der Sman R G M and Boom R M 2006 Lattice Boltzmann simulations of droplet formation in a T-shaped microchannel *Langmuir* **22** 4144–52
[92] Bird G A 1989 Perception of numerical methods in rarefied gasdynamics *Rarefied Gas Dynamics: Theoretical and Computational Techniques* (AIAA) pp 211–26
[93] Liou W W and Fang Y 2001 Heat transfer in microchannel devices using DSMC *J. Microelectromech. Syst.* **10** 274–9
[94] Prasanth P S and Kakkassery J K 2006 Direct simulation Monte Carlo (DSMC): a numerical method for transition-regime flows-a review *J. Indian Inst. Sci.* **86** 169–92
[95] Plotnikov M Y and Shkarupa E V 2014 Theoretical and numerical analysis of approaches to evaluation of statistical error of the DSMC method *Comput. Fluids* **105** 251–61
[96] Bird G A 1976 Molecular gas dynamics *NASA STI/Recon Technical Report A* vol 76 p 40225
[97] Wang M R and Li Z X 2003 Nonideal gas flow and heat transfer in micro-and nanochannels using the direct simulation Monte Carlo method *Phys. Rev.* E **68** 046704
[98] Wang M and Li Z 2004 Simulations for gas flows in microgeometries using the direct simulation Monte Carlo method *Int. J. Heat Fluid Flow* **25** 975–85
[99] Kawagoe Y, Oshima T, Tomarikawa K, Tokumasu T, Koido T and Yonemura S 2016 A study on pressure-driven gas transport in porous media: from nanoscale to microscale *Microfluid. Nanofluid.* **20** 162
[100] Stroock A D, Dertinger S K W, Ajdari A, Mezic I, Stone H A and Whitesides G M 2002 Chaotic mixer for microchannels *Science* **295** 647–51
[101] Shang L R, Cheng Y and Zhao Y J 2017 Emerging droplet microfluidics *Chem. Rev.* **117** 7964–8040
[102] Zhang D Y, Xing W Q, Li W R, Liu S M, Dong Y L, Zhang L C, Zhao F Z, Wang J and Xu Z 2022 Fabrication of multiple parallel microchannels in a single microgroove via the heating assisted MIMIC technique *Micromachines* **13** 364
[103] Bhatia S N and Ingber D E 2014 Microfluidic organs-on-chips *Nat. Biotechnol.* **32** 760–72
[104] Unger M A, Chou H P, Thorsen T, Scherer A and Quake S R 2000 Monolithic microfabricated valves and pumps by multilayer soft lithography *Science* **288** 113–6
[105] Mertaniemi H, Jokinen V, Sainiemi L, Franssila S, Marmur A, Ikkala O and Ras R H A 2011 Superhydrophobic tracks for low-friction, guided transport of water droplets *Adv. Mater.* **23** 2911–4
[106] Ewinger A, Rinke G, Urban A and Kerschbaum S 2013 In situ measurement of the temperature of water in microchannels using laser Raman spectroscopy *Chem. Eng. J.* **223** 129–34
[107] Wu D *et al* 2023 Temperature-regulated bidirectional capillary force self-assembly of femtosecond laser printed micropillars for switchable chiral microstructures *ACS Nano* **17** 12820–8
[108] Zhang W X, Hou W Y, Deike L and Arnold C 2022 Understanding the Rayleigh instability in humping phenomenon during laser powder bed fusion process *Int. J. Extrem. Manuf.* **4** 015201
[109] Yong J L, Yang Q, Huo J L, Hou X and Chen F 2022 Underwater gas self-transportation along femtosecond laser-written open superhydrophobic surface microchannels (<100 μm) for bubble/gas manipulation *Int. J. Extrem. Manuf.* **4** 015002
[110] Enrico A, Voulgaris D, Östmans R, Sundaravadivel N, Moutaux L, Cordier A, Niklaus F, Herland A and Stemme G 2022 3D microvascularized tissue models by laser-based cavitation molding of collagen *Adv. Mater.* **34** 2109823
[111] Das A and Bhaumik S K 2018 Fabrication of cylindrical superhydrophobic microchannels by replicating lotus leaf structures on internal walls *J. Micromech. Microeng.* **28** 045011
[112] Hakamada M, Asao Y, Kuromura T, Chen Y Q, Kusuda H and Mabuchi M 2007 Fabrication of copper microchannels by the spacer method *Scr. Mater.* **56** 781–3
[113] Abbyad P, Dangla R, Alexandrou A and Baroud C N 2011 Rails and anchors: guiding and trapping droplet microreactors in two dimensions *Lab Chip* **11** 813–21
[114] Lathia R and Sen P 2022 JMEMS letters fabrication of self-sealed circular microfluidic channels in glass by thermal blowing method *J. Microelectromech. Syst.* **31** 177–9
[115] Palko J W *et al* 2017 Extreme two-phase cooling from laser-etched diamond and conformal,

template-fabricated microporous copper *Adv. Funct. Mater.* **27** 1703265
[116] Yao P, Schneider G J and Prather D W 2005 Three-dimensional lithographical fabrication of microchannels *J. Microelectromech. Syst.* **14** 799–805
[117] Pisignano D, Sariconi E, Mazzeo M, Gigli G and Cingolani R 2002 High-temperature microfluidic lithography *Adv. Mater.* **14** 1565–7
[118] Albota M *et al* 1998 Design of organic molecules with large two-photon absorption cross sections *Science* **281** 1653–6
[119] Ovsianikov A *et al* 2008 Ultra-low shrinkage hybrid photosensitive material for two-photon polymerization microfabrication *ACS Nano* **2** 2257–62
[120] Yap H K, Ng H Y and Yeow C H 2016 High-force soft printable pneumatics for soft robotic applications *Soft Robot.* **3** 144–58
[121] Castiaux A D, Pinger C W, Hayter E A, Bunn M E, Martin R S and Spence D M 2019 PolyJet 3D-printed enclosed microfluidic channels without photocurable supports *Anal. Chem.* **91** 6910–7
[122] Liao Y B, Li W H, Zhan Z H, Duan H G, Liu P, Chen Y Q and Wang Z L 2021 3D-printed complex microstructures with a self-sacrificial structure enabled by grayscale polymerization and ultrasonic treatment *ACS Omega* **6** 18281–8
[123] Rohbeck N, Ramachandramoorthy R, Casari D, Schürch P, Edwards T E J, Schilinsky L, Philippe L, Schwiedrzik J and Michler J 2020 Effect of high strain rates and temperature on the micromechanical properties of 3D-printed polymer structures made by two-photon lithography *Mater. Des.* **195** 108977
[124] Lyu Z, Wang J L and Chen Y F 2023 4D printing: interdisciplinary integration of smart materials, structural design, and new functionality *Int. J. Extrem. Manuf.* **5** 032011
[125] Gale B K, Jafek A R, Lambert C J, Goenner B L, Moghimifam H, Nze U C and Kamarapu S K 2018 A review of current methods in microfluidic device fabrication and future commercialization prospects *Inventions* **3** 60
[126] Niculescu A G, Chircov C, Bîrcă A C and Grumezescu A M 2021 Fabrication and applications of microfluidic devices: a review *Int. J. Mol. Sci.* **22** 2011
[127] Gross B C, Erkal J L, Lockwood S Y, Chen C P and Spence D M 2014 Evaluation of 3D printing and its potential impact on biotechnology and the chemical sciences *Anal. Chem.* **86** 3240–53
[128] Klank H, Kutter J P and Geschke O 2002 CO_2-laser micromachining and back-end processing for rapid production of PMMA-based microfluidic systems *Lab Chip* **2** 242–6
[129] Kim Y, Sohn I B and Noh Y C 2012 Femtosecond laser micro- and nanopatterning of the fused silica tube to enhance capillary effect *Jpn. J. Appl. Phys.* **51** 102703
[130] Bhattacharjee N, Parra-Cabrera C, Kim Y T, Kuo A P and Folch A 2018 Desktop-stereolithography 3D-printing of a poly(dimethylsiloxane)-based material with sylgard-184 properties *Adv. Mater.* **30** 1800001
[131] Qu H W, Han Z Y, Chen Z G, Tang L, Gao C J, Liu K Z, Pan H B, Fu H Y and Ruan C S 2021 Fractal design boosts extrusion-based 3D printing of bone-mimicking radial-gradient scaffolds *Research* **2021** 9892689
[132] Zwahr C, Serey N, Nitschke L, Bischoff C, Rädel U, Meyer A, Zhu P H and Pfleging W 2023 Targeting new ways for large-scale, high-speed surface functionalization using direct laser interference patterning in a roll-to-roll process *Int. J. Extrem. Manuf.* **5** 035006
[133] Zhang Y R, Chen L, Xie M Z, Zhan Z H, Yang D S, Cheng P, Duan H G, Ge Q and Wang Z L 2022 Ultra-fast programmable human-machine interface enabled by 3D printed degradable conductive hydrogel *Mater. Today Phys.* **27** 100794
[134] De Pra M, De Malsche W, Desmet G, Schoenmakers P J and Kok W T 2007 Pillar-structured microchannels for on-chip liquid chromatography: evaluation of the permeability and separation performance *J. Sep. Sci.* **30** 1453–60
[135] Mei F H, Parida P R, Jiang J, Meng W J and Ekkad S V 2008 Fabrication, assembly, and testing of Cu- and Al-based microchannel heat exchangers *J. Microelectromech. Syst.* **17** 869–81
[136] O'Connor J, Punch J, Jeffers N and Stafford J 2015 A comparison between the hydrodynamic characteristics of 3D-printed polymer and etched silicon microchannels *Microfluid. Nanofluid.* **19** 385–94
[137] Prakash S and Kumar S 2015 Fabrication of microchannels: a review *Proc. Inst. Mech. Eng.* B **229** 1273–88
[138] Sun R D, Nakajima A, Fujishima A, Watanabe T and Hashimoto K 2001 Photoinduced surface wettability conversion of ZnO and TiO_2 thin films *J. Phys. Chem.* B **105** 1984–90
[139] Tan S H, Nguyen N T, Chua Y C and Kang T G 2010 Oxygen plasma treatment for reducing hydrophobicity of a sealed polydimethylsiloxane microchannel *Biomicrofluidics* **4** 032204
[140] Abate A R, Lee D, Do T, Holtze C and Weitz D A 2008 Glass coating for PDMS microfluidic channels by sol–gel methods *Lab Chip* **8** 516–8
[141] Leslie D C, Easley C J, Seker E, Karlinsey J M, Utz M, Begley M R and Landers J P 2009 Frequency-specific flow control in microfluidic circuits with passive elastomeric features *Nat. Phys.* **5** 231–5
[142] Kotz F, Mader M, Dellen N, Risch P, Kick A, Helmer D and Rapp B E 2020 Fused deposition modeling of microfluidic chips in polymethylmethacrylate *Micromachines* **11** 873
[143] El-Atab N, Canas J C and Hussain M M 2020 Pressure-driven two-input 3D microfluidic logic gates *Adv. Sci.* **7** 1903027
[144] Wang F, Zhu J M, Hu X J, Chen L F, Zuo Y F, Yang Y, Jiang F H, Sun C J, Zhao W H and Han X T 2021 Rapid nitrate determination with a portable lab-on-chip device based on double microstructured assisted reactors *Lab Chip* **21** 1109–17
[145] Zhang W H, Lin S C, Wang C M, Hu J, Li C, Zhuang Z X, Zhou Y L, Mathies R A and Yang C J 2009 PMMA/PDMS valves and pumps for disposable microfluidics *Lab Chip* **9** 3088–94
[146] C H J *et al* 2022 Honeycomb-like hydrogel microspheres for 3D bulk construction of tumor models *Research* **2022** 9809763
[147] Geng J, Kang Z, Sun Q, Zhang M, Wang P, Li Y, Li J, Su B and Wei Q 2023 Microtubule assists actomyosin to regulate cell nuclear mechanics and chromatin accessibility *Research* **6** 0054
[148] Yu H B and Zhou G Y 2013 Deformable mold based on-demand microchannel fabrication technology *Sens. Actuators* B **183** 40–45
[149] Nguyen T Q and Park W T 2016 Rapid, low-cost fabrication of circular microchannels by air expansion into partially cured polymer *Sens. Actuators* B **235** 302–8
[150] Tang W L, Liu H, Zhu L Y, Shi J P, Li Z, Xiang N and Yang J Q 2019 Fabrication of different microchannels by adjusting the extrusion parameters for sacrificial molds *Micromachines* **10** 544
[151] Wang Z L, Chen L, Chen Y Q, Liu P, Duan H G and Cheng P 2020 3D printed ultrastretchable, hyper-antifreezing conductive hydrogel for sensitive motion and

electrophysiological signal monitoring *Research* **2020** 1426078
[152] Xie M Z, Zhan Z H, Xu W Q, Zhang C and Wang Z L 2023 Water engine enabled by Janus membrane for precisely controllable long-distance micro-boats driving *Mater. Today Phys.* **38** 101246
[153] Wang Z L, Xie M Z, Guo Q, Liao Y B, Zhang C, Chen Y P, Dong Z C and Duan H G 2023 Hyper-anti-freezing bionic functional surface to −90° C *PNAS Nexus* **2** pgad177
[154] Zhang R J and Larsen N B 2017 Stereolithographic hydrogel printing of 3D culture chips with biofunctionalized complex 3D perfusion networks *Lab Chip* **17** 4273–82
[155] Xie M Z, Duan H G, Cheng P, Chen Y P, Dong Z C and Wang Z L 2022 Underwater unidirectional cellular fluidics *ACS Appl. Mater. Interfaces* **14** 9891–8
[156] Wang Z L, Li Y Y, Gong S, Li W H, Duan H G, Cheng P, Chen Y P and Dong Z C 2022 Three-dimensional open water microchannel transpiration mimetics *ACS Appl. Mater. Interfaces* **14** 30435–42
[157] Li C X, Dai H Y, Gao C, Wang T, Dong Z C and Jiang L 2019 Bioinspired inner microstructured tube controlled capillary rise *Proc. Natl Acad. Sci. USA* **116** 12704–9
[158] Wang Z L, Zhan Z H, Chen L, Duan G H, Cheng P, Kong H, Chen Y P and Duan H G 2022 3D-printed bionic solar evaporator *Sol. RRL* **6** 2101063
[159] Zhan Z H, Chen L, Wang C, Shuai Y, Duan H G and Wang Z L 2023 Super water-storage self-adhesive gel for solar vapor generation and collection *ACS Appl. Mater. Interfaces* **15** 8181–9
[160] Bertassoni L E *et al* 2014 Hydrogel bioprinted microchannel networks for vascularization of tissue engineering constructs *Lab Chip* **14** 2202–11
[161] Gao Q, He Y, Fu J Z, Liu A and Ma L 2015 Coaxial nozzle-assisted 3D bioprinting with built-in microchannels for nutrients delivery *Biomaterials* **61** 203–15
[162] Chen H X, Bian F K, Guo J H and Zhao Y J 2022 Aptamer-functionalized barcodes in herringbone microfluidics for multiple detection of exosomes *Small Methods* **6** 2200236
[163] Wang C, Wang J L, Zhang Z H, Wang Q and Shang L R 2023 DNA–polyelectrolyte composite responsive microparticles for versatile chemotherapeutics cleaning *Research* **6** 0083
[164] Askari M, Afzali Naniz M, Kouhi M, Saberi A, Zolfagharian A and Bodaghi M 2021 Recent progress in extrusion 3D bioprinting of hydrogel biomaterials for tissue regeneration: a comprehensive review with focus on advanced fabrication techniques *Biomater. Sci.* **9** 535–73
[165] Lu B T, Hu E L, Ding W W, Wang W Y, Xie R Q, Yu K, Lu F, Lan G Q and Dai F Y 2023 Bioinspired hemostatic strategy via pulse ejections for severe bleeding wounds *Research* **6** 0150
[166] Duan X F, Huang Y, Agarwal R and Lieber C M 2003 Single-nanowire electrically driven lasers *Nature* **421** 241–5
[167] Morales A M and Lieber C M 1998 A laser ablation method for the synthesis of crystalline semiconductor nanowires *Science* **279** 208–11
[168] Wang Z L, Quan X J, Yao W, Wang L and Cheng P 2016 Plasma resonance effects on bubble nucleation in flow boiling of a nanofluid irradiated by a pulsed laser beam *Int. Commun. Heat Mass Transfer* **72** 90–94
[169] Wang Z L and Cheng P 2019 Enhancements of absorption and photothermal conversion of solar energy enabled by surface plasmon resonances in nanoparticles and metamaterials *Int. J. Heat Mass Transfer* **140** 453–82
[170] Wang Z L, Yang P Y, Qi G G, Zhang Z M and Cheng P 2020 An experimental study of a nearly perfect absorber made from a natural hyperbolic material for harvesting solar energy *J. Appl. Phys.* **127** 233102
[171] Liu X F, Guo Q B and Qiu J R 2017 Emerging low-dimensional materials for nonlinear optics and ultrafast photonics *Adv. Mater.* **29** 1605886
[172] Suk J W, Lee W H, Lee J, Chou H, Piner R D, Hao Y F, Akinwande D and Ruoff R S 2013 Enhancement of the electrical properties of graphene grown by chemical vapor deposition via controlling the effects of polymer residue *Nano Lett.* **13** 1462–7
[173] Xue J J, Wu T, Dai Y Q and Xia Y N 2019 Electrospinning and electrospun nanofibers: methods, materials, and applications *Chem. Rev.* **119** 5298–415
[174] Gattass R R and Mazur E 2008 Femtosecond laser micromachining in transparent materials *Nat. Photon.* **2** 219–25
[175] Goulielmakis E *et al* 2008 Single-cycle nonlinear optics *Science* **320** 1614–7
[176] Sundaram S K and Mazur E 2002 Inducing and probing non-thermal transitions in semiconductors using femtosecond laser pulses *Nat. Mater.* **1** 217–24
[177] Chen C, Shi L A, Huang Z C, Hu Y L, Wu S Z, Li J W, Wu D and Chu J R 2019 Microhole-arrayed PDMS with controllable wettability gradient by one-step femtosecond laser drilling for ultrafast underwater bubble unidirectional self-transport *Adv. Mater. Interfaces* **6** 1900297
[178] Wiedemeier S, Römer R, Wächter S, Staps U, Kolbe C and Gastrock G 2017 Precision moulding of biomimetic disposable chips for droplet-based applications *Microfluid. Nanofluid.* **21** 167
[179] Qu P, Lei J P, Sheng J, Zhang L and Ju H X 2011 Simultaneous multiple enantioseparation with a one-pot imprinted microfluidic channel by microchip capillary electrochromatography *Analyst* **136** 920–6
[180] Trappmann B *et al* 2012 Extracellular-matrix tethering regulates stem-cell fate *Nat. Mater.* **11** 642–9
[181] Kolesky D B, Truby R L, Gladman A S, Busbee T A, Homan K A and Lewis J A 2014 3D bioprinting of vascularized, heterogeneous cell-laden tissue constructs *Adv. Mater.* **26** 3124–30
[182] Hammock M L, Chortos A, Tee B C K, Tok J B H and Bao Z A 2013 25th anniversary article: the evolution of electronic skin (E-skin): a brief history, design considerations, and recent progress *Adv. Mater.* **25** 5997–6038
[183] Li Y L, Rodrigues J and Tomás H 2012 Injectable and biodegradable hydrogels: gelation, biodegradation and biomedical applications *Chem. Soc. Rev.* **41** 2193–221
[184] Guo L J 2007 Nanoimprint lithography: methods and material requirements *Adv. Mater.* **19** 495–513
[185] Gates B D, Xu Q B, Stewart M, Ryan D, Willson C G and Whitesides G M 2005 New approaches to nanofabrication: molding, printing, and other techniques *Chem. Rev.* **105** 1171–96
[186] Ueno K, Kitagawa F and Kitamura N 2002 Photocyanation of pyrene across an oil/water interface in a polymer microchannel chip *Lab Chip* **2** 231–4
[187] Beebe D J, Moore J S, Bauer J M, Yu Q, Liu R H, Devadoss C and Jo B H 2000 Functional hydrogel structures for autonomous flow control inside microfluidic channels *Nature* **404** 588–90
[188] Ozcelik A, Ahmed D, Xie Y L, Nama N, Qu Z G, Nawaz A A and Huang T J 2014 An acoustofluidic micromixer via bubble inception and cavitation from microchannel sidewalls *Anal. Chem.* **86** 5083–8
[189] Liu G, Tian Y and Zhang X 2003 Fabrication of microchannels in negative resist *Microsyst. Technol.* **9** 461–4
[190] Grigorescu A E and Hagen C W 2009 Resists for sub-20-nm electron beam lithography with a focus on HSQ: state of the art *Nanotechnology* **20** 292001

[191] Hnatovsky C, Taylor R S, Simova E, Rajeev P P, Rayner D M, Bhardwaj V R and Corkum P B 2006 Fabrication of microchannels in glass using focused femtosecond laser radiation and selective chemical etching *Appl. Phys.* A **84** 47–61

[192] Goldman J L, Long B R, Gewirth A A and Nuzzo R G 2011 Strain anisotropies and self-limiting capacities in single-crystalline 3D silicon microstructures: models for high energy density lithium-ion battery anodes *Adv. Funct. Mater.* **21** 2412–22

[193] Zhuang D and Edgar J H 2005 Wet etching of GaN, AlN, and SiC: a review *Mater. Sci. Eng.* R **48** 1–46

[194] Rinzler A G, Hafner J H, Nikolaev P, Nordlander P, Colbert D T, Smalley R E, Lou L, Kim S G and Tománek D 1995 Unraveling nanotubes: field emission from an atomic wire *Science* **269** 1550–3

[195] Huang Z P, Geyer N, Werner P, de Boor J and Gösele U 2011 Metal-assisted chemical etching of silicon: a review *Adv. Mater.* **23** 285–308

[196] Yang R, Zhang L C, Wang Y, Shi Z W, Shi D X, Gao H J, Wang E G and Zhang G Y 2010 An anisotropic etching effect in the graphene basal plane *Adv. Mater.* **22** 4014–9

[197] Whitby M and Quirke N 2007 Fluid flow in carbon nanotubes and nanopipes *Nat. Nanotechnol.* **2** 87–94

[198] Zeng H J, Wan Z L and Feinerman A D 2006 Fabrication of micro/nano fluidic channels with sacrificial galvanic coupled metals *Nanotechnology* **17** 3183–8

[199] Song K H, Highley C B, Rouff A and Burdick J A 2018 Complex 3D-printed microchannels within cell-degradable hydrogels *Adv. Funct. Mater.* **28** 1801331

[200] Mazzoli A 2013 Selective laser sintering in biomedical engineering *Med. Biol. Eng. Comput.* **51** 245–56

[201] Goh W H and Hashimoto M 2018 Fabrication of 3D microfluidic channels and in-channel features using 3D printed, water-soluble sacrificial mold *Macromol. Mater. Eng.* **303** 1700484

[202] Lewis J A 2006 Direct ink writing of 3D functional materials *Adv. Funct. Mater.* **16** 2193–204

[203] He X, Lin Y C, Ding Y C, Abdullah A M, Lei Z P, Han Y B, Shi X J, Zhang W and Yu K 2022 Reshapeable, rehealable and recyclable sensor fabricated by direct ink writing of conductive composites based on covalent adaptable network polymers *Int. J. Extrem. Manuf.* **4** 015301

[204] Zhou W H, Kuebler S M, Braun K L, Yu T Y, Cammack J K, Ober C K, Perry J W and Marder S R 2002 An efficient two-photon-generated photoacid applied to positive-tone 3D microfabrication *Science* **296** 1106–9

[205] Zou M Q *et al* 2023 3D printed fiber-optic nanomechanical bioprobe *Int. J. Extrem. Manuf.* **5** 015005

[206] Gopinathan J and Noh I 2018 Recent trends in bioinks for 3D printing *Biomater. Res.* **22** 11

[207] Hu S Q, Huan X, Liu Y, Cao S X, Wang Z R and Kim J T 2023 Recent advances in meniscus-on-demand three-dimensional micro- and nano-printing for electronics and photonics *Int. J. Extrem. Manuf.* **5** 032009

[208] Luo M J, Li R D, Zheng D, Kang J T, Wu H T, Deng S H and Niu P D 2023 Formation mechanism of inherent spatial heterogeneity of microstructure and mechanical properties of NiTi SMA prepared by laser directed energy deposition *Int. J. Extrem. Manuf.* **5** 035005

[209] Wallin T J, Pikul J and Shepherd R F 2018 3D printing of soft robotic systems *Nat. Rev. Mater.* **3** 84–100

[210] Gouzman I, Grossman E, Verker R, Atar N, Bolker A and Eliaz N 2019 Advances in polyimide-based materials for space applications *Adv. Mater.* **31** 1807738

[211] Knowlton S, Yu C H, Ersoy F, Emadi S, Khademhosseini A and Tasoglu S 2016 3D-printed microfluidic chips with patterned, cell-laden hydrogel constructs *Biofabrication* **8** 025019

[212] Patel D K, Sakhaei A H, Layani M, Zhang B, Ge Q and Magdassi S 2017 Highly stretchable and UV curable elastomers for digital light processing based 3D printing *Adv. Mater.* **29** 1606000

[213] Liu Z X, Zhan Z D, Shen T, Li N, Zhang C Q, Yu C L, Li C X, Si Y F, Jiang L and Dong Z C 2023 Dual-bionic superwetting gears with liquid directional steering for oil-water separation *Nat. Commun.* **14** 4128

[214] Kawata S, Sun H B, Tanaka T and Takada K 2001 Finer features for functional microdevices *Nature* **412** 697–8

[215] Schizas C, Melissinaki V, Gaidukeviciute A, Reinhardt C, Ohrt C, Dedoussis V, Chichkov B N, Fotakis C, Farsari M and Karalekas D 2010 On the design and fabrication by two-photon polymerization of a readily assembled micro-valve *Int. J. Adv. Manuf. Technol.* **48** 435–41

[216] Capel A J, Edmondson S, Christie S D R, Goodridge R D, Bibb R J and Thurstans M 2013 Design and additive manufacture for flow chemistry *Lab Chip* **13** 4583–90

[217] Abayazid F F and Ghajari M 2020 Material characterisation of additively manufactured elastomers at different strain rates and build orientations *Addit. Manuf.* **33** 101160

[218] Chen L, Wang Z L, Zhan Z H, Xie M Z, Duan G H, Cheng P, Chen Y Q and Duan H G 2021 3D printed super-anti-freezing self-adhesive human-machine interface *Mater. Today Phys.* **19** 100404

[219] Zhang W Q, Ye H T, Feng X B, Zhou W Z, Cao K, Li M Y, Fan S F and Lu Y 2022 Tailoring mechanical properties of PμSL 3D-printed structures via size effect *Int. J. Extrem. Manuf.* **4** 045201

[220] Moss D J, Morandotti R, Gaeta A L and Lipson M 2013 New CMOS-compatible platforms based on silicon nitride and Hydex for nonlinear optics *Nat. Photon.* **7** 597–607

[221] Zhou W, Deng W J, Lu L S, Zhang J P, Qin L F, Ma S L and Tang Y 2014 Laser micro-milling of microchannel on copper sheet as catalyst support used in microreactor for hydrogen production *Int. J. Hydrog. Energy* **39** 4884–94

[222] Deng D X, Wan W, Shao H R, Tang Y, Feng J Y and Zeng J 2015 Effects of operation parameters on flow boiling characteristics of heat sink cooling systems with reentrant porous microchannels *Energy Convers. Manage* **96** 340–51

[223] Kaur G, Tomar M and Gupta V 2018 Development of a microfluidic electrochemical biosensor: prospect for point-of-care cholesterol monitoring *Sens. Actuators* B **261** 460–6

[224] Abdelgawad M, Wu C, Chien W Y, Geddie W R, Jewett M A S and Sun Y 2011 A fast and simple method to fabricate circular microchannels in polydimethylsiloxane (PDMS) *Lab Chip* **11** 545–51

[225] Fukuba T, Yamamoto T, Naganuma T and Fujii T 2004 Microfabricated flow-through device for DNA amplification—towards in situ gene analysis *Chem. Eng. J.* **101** 151–6

[226] Siemsen K, Rajput S, Rasch F, Taheri F, Adelung R, Lammerding J and Selhuber-Unkel C 2021 Tunable 3D hydrogel microchannel networks to study confined mammalian cell migration *Adv. Healthcare Mater.* **10** 2100625

[227] Cao Q H, Gao Y, Pu J, Zhao X, Wang Y X, Chen J P and Guan C 2023 Gradient design of imprinted anode for stable Zn-ion batteries *Nat. Commun.* **14** 641

[228] Atwater J, Mattes D S, Streit B, von Bojničić-kninski C, Loeffler F F, Breitling F, Fuchs H and Hirtz M 2018 Combinatorial synthesis of macromolecular arrays by microchannel cantilever spotting (μCS) *Adv. Mater.* **30** 1801632

[229] Levato R *et al* 2021 High-resolution lithographic biofabrication of hydrogels with complex microchannels

from low-temperature-soluble gelatin bioresins *Mater. Today Bio* **12** 100162
[230] Trebbin M, Steinhauser D, Perlich J, Buffet A, Roth S V, Zimmermann W, Thiele J and Förster S 2013 Anisotropic particles align perpendicular to the flow direction in narrow microchannels *Proc. Natl Acad. Sci. USA* **110** 6706–11
[231] Wu Y Y, Gu Y W, Kang W D, Yu H T, Chen S, Quan X and Lu N 2023 Construction of microchannel charcoal cathodes with spatial-constraint capability for enhancing reduction of NO_3^- in high-salinity water *Chem. Eng. J.* **452** 139126
[232] Li L K, Zhang Y N, Zhou Y F, Zheng W L, Sun Y T, Ma G M and Zhao Y 2021 Optical fiber optofluidic bio-chemical sensors: a review *Laser Photonics Rev.* **15** 2000526
[233] Quero R F, de Castro Costa B M, da Silva J A F and de Jesus D P 2022 Using multi-material fused deposition modeling (FDM) for one-step 3D printing of microfluidic capillary electrophoresis with integrated electrodes for capacitively coupled contactless conductivity detection *Sens. Actuators* B **365** 131959
[234] Ali M A, Hu C S, Yttri E A and Panat R 2022 Recent advances in 3D printing of biomedical sensing devices *Adv. Funct. Mater.* **32** 2107671
[235] Messelmani T, Morisseau L, Sakai Y, Legallais C, Le Goff A, Leclerc E and Jellali R 2022 Liver organ-on-chip models for toxicity studies and risk assessment *Lab Chip* **22** 2423–50
[236] Su R T, Wen J X, Su Q, Wiederoder M S, Koester S J, Uzarski J R and McAlpine M C 2020 3D printed self-supporting elastomeric structures for multifunctional microfluidics *Sci. Adv.* **6** eabc9846
[237] Guo Y B, Shahsavan H and Sitti M 2020 3D microstructures of liquid crystal networks with programmed voxelated director fields *Adv. Mater.* **32** 2002753
[238] Lichade K M, Hu S and Pan Y Y 2023 Acoustic streaming-assisted two-photon polymerization process for the production of multimaterial microstructures *Addit. Manuf.* **70** 103552
[239] Hsu C T and Cheng P 1990 Thermal dispersion in a porous medium *Int. J. Heat Mass Transfer* **33** 1587–97
[240] Hamida M B B and Hatami M 2021 Optimization of fins arrangements for the square light emitting diode (LED) cooling through nanofluid-filled microchannel *Sci. Rep.* **11** 12610
[241] van Erp R, Soleimanzadeh R, Nela L, Kampitsis G and Matioli E 2020 Co-designing electronics with microfluidics for more sustainable cooling *Nature* **585** 211–6
[242] Wang G D, Cheng P and Bergles A E 2008 Effects of inlet/outlet configurations on flow boiling instability in parallel microchannels *Int. J. Heat Mass Transfer* **51** 2267–81
[243] Quan X J, Cheng P and Wu H Y 2008 Transition from annular flow to plug/slug flow in condensation of steam in microchannels *Int. J. Heat Mass Transfer* **51** 707–16
[244] Qu J, Wu H Y and Cheng P 2010 Thermal performance of an oscillating heat pipe with Al_2O_3–water nanofluids *Int. Commun. Heat Mass Transfer* **37** 111–5
[245] Drummond K P, Back D, Sinanis M D, Janes D B, Peroulis D, Weibel J A and Garimella S V 2018 A hierarchical manifold microchannel heat sink array for high-heat-flux two-phase cooling of electronics *Int. J. Heat Mass Transfer* **117** 319–30
[246] Zhou J H, Chen X M, Zhao Q, Lu M X, Hu D H and Li Q 2021 Flow thermohydraulic characterization of hierarchical-manifold microchannel heat sink with uniform flow distribution *Appl. Therm. Eng.* **198** 117510
[247] Wang T H, Wu H C, Meng J H and Yan W M 2020 Optimization of a double-layered microchannel heat sink with semi-porous-ribs by multi-objective genetic algorithm *Int. J. Heat Mass Transfer* **149** 119217
[248] Zeng S and Lee P S 2019 Topology optimization of liquid-cooled microchannel heat sinks: an experimental and numerical study *Int. J. Heat Mass Transfer* **142** 118401
[249] Wang G, Li Y, Qiu H H, Yan H and Zhou Y G 2023 High-performance and wide relative humidity passive evaporative cooling utilizing atmospheric water *Droplet* **2** e32
[250] Chen Y P, Gao W, Zhang C B and Zhao Y J 2016 Three-dimensional splitting microfluidics *Lab Chip* **16** 1332–9
[251] Yang X L, Qi B, Lu Y, Zhang W and Wang X L 2023 Bionic surface diode for droplet steering *Droplet* **2** e46
[252] Zhang Q Y, Li Y, Yan Y F, Zhang X F, Tian D L and Jiang L 2020 Highly flexible monolayered porous membrane with superhydrophilicity-hydrophilicity for unidirectional liquid penetration *ACS Nano* **14** 7287–96
[253] Hu S T, Cao X B, Reddyhoff T, Ding X J, Shi X, Dini D, Demello A J, Peng Z K and Wang Z K 2022 Pneumatic programmable superrepellent surfaces *Droplet* **1** 48–55
[254] Zhan Z H, Wang Z L, Xie M Z, Chen Y P and Hui H G 2024 Programmable droplet bouncing on bionic functional surfaces for continuous electricity generation *Adv. Funct. Mater.* **34** 2304520
[255] Yin Y R, Zhu C Y, Fu T T, Ma Y G, Wang K and Luo G S 2019 Enhancement effect and mechanism of gas-liquid mass transfer by baffles embedded in the microchannel *Chem. Eng. Sci.* **201** 264–73
[256] Caggioni M, Traini D, Young P M and Spicer P T 2018 Microfluidic production of endoskeleton droplets with controlled size and shape *Powder Technol.* **329** 129–36
[257] Wang Z L, Liu Z, Duan G H, Fang L Y and Duan H G 2022 Ultrahigh broadband absorption in metamaterials with electric and magnetic polaritons enabled by multiple materials *Int. J. Heat Mass Transfer* **185** 122355
[258] Wang Z L, Zhang Z M, Quan X J and Cheng P 2018 A numerical study on effects of surrounding medium, material, and geometry of nanoparticles on solar absorption efficiencies *Int. J. Heat Mass Transfer* **116** 825–32
[259] Wang Z L, Quan X J, Zhang Z M and Cheng P 2018 Optical absorption of carbon-gold core-shell nanoparticles *J. Quant. Spectrosc. Radiat. Transfer* **205** 291–8
[260] Wang Z L, Zhang Z M, Quan X J and Cheng P 2018 A perfect absorber design using a natural hyperbolic material for harvesting solar energy *Sol. Energy* **159** 329–36
[261] Liu Z, Duan G H, Duan H G and Wang Z L 2022 Nearly perfect absorption of solar energy by coherent of electric and magnetic polaritons *Sol. Energy Mater. Sol. Cells* **240** 111688
[262] Wang Z L, Liu Z, Zhang C, Yang D S, Cheng P and Shuai Y 2022 Notched nanoring wideband absorber for total solar energy harvesting *Sol. Energy* **243** 153–62
[263] Fan X Q, Yang Y, Shi X L, Liu Y, Li H P, Liang J J and Chen Y S 2020 A MXene-based hierarchical design enabling highly efficient and stable solar-water desalination with good salt resistance *Adv. Funct. Mater.* **30** 2007110
[264] Lin J B, Tan X H, Shi T L, Tang Z R and Liao G L 2018 Leaf vein-inspired hierarchical wedge-shaped tracks on flexible substrate for enhanced directional water collection *ACS Appl. Mater. Interfaces* **10** 44815–24
[265] Liu C, Hong K, Sun X, Natan A, Luan P C, Yang Y and Zhu H L 2020 An 'antifouling' porous loofah sponge with internal microchannels as solar absorbers and water

pumpers for thermal desalination *J. Mater. Chem.* A **8** 12323–33
[266] Dudukovic N A, Fong E J, Gemeda H B, Deotte J R, Cerón M R, Moran B D, Davis J T, Baker S E and Duoss E B 2021 Cellular fluidics *Nature* **595** 58–65
[267] Zhang H T, Li L, He N, Wang H N, Wang B S, Dong T Y, Jiang B and Tang D W 2022 Bioinspired hierarchical evaporator via cell wall engineering for highly efficient and sustainable solar desalination *EcoMat* **4** e12216
[268] Cheng S W, Sun Z H, Wu Y, Gao P, He J X, Yin Z Y, Liu L Y and Li G 2021 A thermally insulated solar evaporator coupled with a passive condenser for freshwater collection *J. Mater. Chem.* A **9** 22428–39
[269] Ma J X *et al* 2022 A light-permeable solar evaporator with three-dimensional photocatalytic sites to boost volatile-organic-compound rejection for water purification *Environ. Sci. Technol.* **56** 9797–805
[270] Ge X H, Huang X L, Huang S Z, Zhang H F, Wang X D, Ye C S, Qiu T and Xu K 2022 Enhanced solvent extraction in a serial converging-diverging microchannel at high injection ratio *Chem. Eng. Sci.* **259** 117845
[271] Zhu Q Y, Xu Y N, Qiu L, Ma C C, Yu B W, Song Q, Jin W, Jin Q H, Liu J Y and Mu Y 2017 A scalable self-priming fractal branching microchannel net chip for digital PCR *Lab Chip* **17** 1655–65
[272] Olanrewaju A O, Robillard A, Dagher M and Juncker D 2016 Autonomous microfluidic capillaric circuits replicated from 3D-printed molds *Lab Chip* **16** 3804–14
[273] Farmehini V, Kiendzior S, Landers J P and Swami N S 2021 Real-time detection and control of microchannel resonance frequency in acoustic trapping systems by monitoring amplifier supply currents *ACS Sens.* **6** 3765–72
[274] Hu B F, Li J J, Mou L, Liu Y, Deng J Q, Qian W, Sun J S, Cha R T and Jiang X Y 2017 An automated and portable microfluidic chemiluminescence immunoassay for quantitative detection of biomarkers *Lab Chip* **17** 2225–34
[275] Song C L, Jin T, Yan R P, Qi W Z, Huang T Y, Ding H F, Tan S H, Nguyen N T and Xi L 2018 Opto-acousto-fluidic microscopy for three-dimensional label-free detection of droplets and cells in microchannels *Lab Chip* **18** 1292–7
[276] Pinho D, Yaginuma T and Lima R 2013 A microfluidic device for partial cell separation and deformability assessment *BioChip J.* **7** 367–74
[277] Rodrigues R O, Pinho D, Faustino V and Lima R 2015 A simple microfluidic device for the deformability assessment of blood cells in a continuous flow *Biomed. Microdev.* **17** 108
[278] Mane N S, Puri D B, Mane S, Hemadri V, Banerjee A and Tripathi S 2022 Separation of motile human sperms in a T-shaped sealed microchannel *Biomed. Eng. Lett.* **12** 331–42
[279] Jiang Z Y, Zhang K H, Du L L, Cheng Z J, Zhang T X, Ding J, Li W, Xu B S and Zhu M F 2021 Construction of chitosan scaffolds with controllable microchannel for tissue engineering and regenerative medicine *Mater. Sci. Eng.* C **126** 112178
[280] Vu-Dinh H, Do Quang L, Chang C C, Nhu C N, Thanh H T, Bui T T, Duc T C and Jen C P 2021 Immunomagnetic separation in a novel cavity-added serpentine microchannel structure for the selective isolation of lung adenocarcinoma cells *Biomed. Microdev.* **23** 51
[281] Tee C A, Yang Z, Yin L, Wu Y N, Han J and Lee E H 2019 Improved zonal chondrocyte production protocol integrating size-based inertial spiral microchannel separation and dynamic microcarrier culture for clinical application *Biomaterials* **220** 119409
[282] Oh S and Choi S 2018 3D-printed capillary circuits for calibration-free viscosity measurement of Newtonian and non-Newtonian fluids *Micromachines* **9** 314
[283] Yafia M, Ymbern O, Olanrewaju A O, Parandakh A, Sohrabi Kashani A, Renault J, Jin Z J, Kim G, Ng A and Juncker D 2022 Microfluidic chain reaction of structurally programmed capillary flow events *Nature* **605** 464–9
[284] Safavieh R and Juncker D 2013 Capillarics: pre-programmed, self-powered microfluidic circuits built from capillary elements *Lab Chip* **13** 4180
[285] Zang Y P, Zhang F J, Huang D Z, Gao X K, Di C A and Zhu D B 2015 Flexible suspended gate organic thin-film transistors for ultra-sensitive pressure detection *Nat. Commun.* **6** 6269
[286] Zhang F J, Zang Y P, Huang D Z, Di C A and Zhu D B 2015 Flexible and self-powered temperature-pressure dual-parameter sensors using microstructure-frame-supported organic thermoelectric materials *Nat. Commun.* **6** 8356
[287] Debener S, Emkes R, De Vos M and Bleichner M 2015 Unobtrusive ambulatory EEG using a smartphone and flexible printed electrodes around the ear *Sci. Rep.* **5** 16743
[288] Ahmed D, Sukhov A, Hauri D, Rodrigue D, Maranta G, Harting J and Nelson B J 2021 Bioinspired acousto-magnetic microswarm robots with upstream motility *Nat. Mach. Intell.* **3** 116–24
[289] Milana E, Gorissen B, Peerlinck S, De Volder M and Reynaerts D 2019 Artificial soft cilia with asymmetric beating patterns for biomimetic low-Reynolds-number fluid propulsion *Adv. Funct. Mater.* **29** 1900462
[290] Zhao C *et al* 2021 A high-energy and long-cycling lithium–sulfur pouch cell via a macroporous catalytic cathode with double-end binding sites *Nat. Nanotechnol.* **16** 166–73
[291] Luo Y, Li K, Chen Y T, Feng J Z, Wang L K, Jiang Y G, Li L J, Yu G and Feng J 2023 Single -atom and hierarchical-pore aerogel confinement strategy for low-platinum fuel cells *Adv. Mater.* **35** 2300624
[292] Braff W A, Bazant M Z and Buie C R 2013 Membrane-less hydrogen bromine flow battery *Nat. Commun.* **4** 2346
[293] Yameen B, Kaltbeitzel A, Langer A, Müller F, Gösele U, Knoll W and Azzaroni O 2009 Highly proton-conducting self-humidifying microchannels generated by copolymer brushes on a scaffold *Angew. Chem., Int. Ed.* **48** 3124–8
[294] Wang Z L, Xiong J S, Liao Y B, Xie M Z, Yang D S, Zhang C, Chen Y P and Zou Z G 2023 Bionic Janus membranes to manipulate bubbles underwater for hydrogen evolution reactions *Chem. Eng. J.* **474** 145352
[295] Bombelli P *et al* 2011 Quantitative analysis of the factors limiting solar power transduction by *Synechocystis sp*. PCC. 6803 in biological photovoltaic devices *Energy Environ. Sci.* **4** 4690
[296] Yang Y, Li T, Feng P Z, Wang X X, Wang S R, Ling Y H and Shao Z P 2022 Highly efficient conversion of oxygen-bearing low concentration coal-bed methane into power via solid oxide fuel cell integrated with an activated catalyst-modified anode microchannel *Appl. Energy* **328** 120134
[297] Zhao T S, Xu C, Chen R and Yang W W 2009 Mass transport phenomena in direct methanol fuel cells *Prog. Energy Combust. Sci.* **35** 275–92
[298] Zhao T S, Yang W W, Chen R and Wu Q X 2010 Towards operating direct methanol fuel cells with highly concentrated fuel *J. Power Sources* **195** 3451–62
[299] deMello A J 2006 Control and detection of chemical reactions in microfluidic systems *Nature* **442** 394–402
[300] Chai M, Razavi Bazaz S, Daiyan R, Razmjou A, Ebrahimi Warkiani M, Amal R and Chen V 2021 Biocatalytic micromixer coated with enzyme-MOF thin film for CO_2 conversion to formic acid *Chem. Eng. J.* **426** 130856

[301] Brooks K P, Hu J L, Zhu H Y and Kee R J 2007 Methanation of carbon dioxide by hydrogen reduction using the Sabatier process in microchannel reactors *Chem. Eng. Sci.* **62** 1161–70

[302] Khani Y, Safari N, Kamyar N, Bahadoran F and Torabi M 2022 High H_2 selectivity with low coke formation for methanol steam reforming over $Cu/Y_{1.5}Ce_{0.84}Ru_{0.04}O_4$ catalyst in a microchannel plate reactor *Int. J. Hydrog. Energy* **47** 971–83

[303] Gribovskiy A G, Makarshin L L, Andreev D V, Klenov O P and Parmon V N 2015 Thermally autonomous microchannel reactor to produce hydrogen in steam reforming of methanol *Chem. Eng. J.* **273** 130–7

[304] Xia Q, Lin L R, Lin Z H, Chen C, Jin W Y and Liu Q B 2022 Development of a Pd-Ag H_2-selective membrane microchannel reactor for efficient solar hydrogen production with ammonia *Energy Convers. Manage.* **270** 116181